This is a repository copy of *Asynchronous carbon sink saturation in African and Amazonian tropical forests*.

White Rose Research Online URL for this paper:
http://eprints.whiterose.ac.uk/158208/

Version: Accepted Version

Article:

1 **Asynchronous Carbon Sink Saturation in African and Amazonian Tropical Forests**

2

3 **Authors**

4 Wannes Hubau[1,2,3]*, Simon L. Lewis[1,4]*, Oliver L. Phillips[1], Kofi Affum-Baffoe[5], Hans Beeckman[2], Aida

5 Cuní-Sanchez[4,6], Armandu K. Daniels[7], Corneille E.N. Ewango[8,9,10], Sophie Fauset[11,1], Jacques M. Mukinzi

6 [8,12,13], Douglas Sheil[14,15,16], Bonaventure Sonké[17], Martin J.P. Sullivan[1,18], Terry C.H. Sunderland[16,19], Hermann

7 Taedoumg[17,20], Sean C. Thomas[21], Lee J.T. White[22,23,24], Katharine A. Abernethy[24,23], Stephen Adu-Bredu[25],

8 Christian A. Amani[26,16], Timothy R. Baker[1], Lindsay F. Banin[27], Fidèle Baya[28,29], Serge K. Begne[17,1], Amy C.

9 Bennett[1], Fabrice Benedet[30,31], Robert Bitariho[15], Yannick E. Bocko[32], Pascal Boeckx[33], Patrick Boundja[34,16,35],

10 Roel J.W. Brienen[1], Terry Brncic[34], Eric Chezeaux[36], George B. Chuyong[37], Connie J. Clark[38], Murray

11 Collins[39,40], James A. Comiskey[41,42], David A. Coomes[43], Greta C. Dargie[1], Thales de Haulleville[2], Marie Noel

12 Djuikouo K.[37], Jean-Louis Doucet[44], Adriane Esquivel-Muelbert[1,45], Ted R. Feldpausch[46], Alusine Fofanah[47],

13 Ernest G. Foli[25], Martin Gilpin[1], Emanuel Gloor[1], Christelle Gonmadje[48], Sylvie Gourlet-Fleury[30,31], Jefferson

14 S. Hall [49], Alan C. Hamilton[50], David J. Harris[51], Terese B. Hart[52,53], Mireille B.N. Hockemba[34], Annette

15 Hladik[54], Suspense A. Ifo[55], Kathryn J. Jeffery[24], Tommaso Jucker[56], Emmanuel Kasongo Yakusu[10,3,2],

16 Elizabeth Kearsley[57,2], David Kenfack[49,58], Alexander Koch[4,59], Miguel E. Leal[60], Aurora Levesley[1], Jeremy A.

17 Lindsell[61,62], Janvier Lisingo[63], Gabriela Lopez-Gonzalez[1], Jon C. Lovett[1,64], Jean-Remy Makana[63], Yadvinder

18 Malhi[65], Andrew R. Marshall[6,66,67], Jim Martin[68], Emanuel H. Martin[58,69], Faustin M. Mbayu[10], Vincent P.

19 Medjibe[70,71,38], Vianet Mihindou[71,22], Edward T.A. Mitchard[39], Sam Moore[65], Pantaleo K.T. Munishi[72],

20 Natacha Nssi Bengone[22], Lucas Ojo[73], Fidèle Evouna Ondo[71], Kelvin Peh[74,75], Georgia C. Pickavance[1], Axel

21 D. Poulsen[51], John R. Poulsen[38], Lan Qie[1,76], Jan Reitsma[77], Francesco Rovero[78,79], Michael D. Swaine[80], Joey

22 Talbot[1], James Taplin[81], David M. Taylor[82], Duncan W. Thomas[83], Benjamin Toirambe[84,2], John Tshibamba

23 Mukendi[2,10,85], Darlington Tuagben[7], Peter M. Umunay[86,87], Geertje M.F. Van Der Heijden[88], Hans

24 Verbeeck[57], Jason Vleminckx[89,90], Simon Willcock[91], Hannsjoerg Woell[92], John T. Woods[93], Lise Zemagho[17]

25

26 *Contributed equally

27

1

Author affiliations

1. University of Leeds, School of Geography, Leeds, UK

2. Royal Museum for Central Africa, Service of Wood Biology, Tervuren, Belgium

3. Ghent University, Department of Environment, Laboratory of Wood Technology (Woodlab), Ghent, Belgium

4. University College London, Department of Geography, London, UK

5. Forestry Commission of Ghana, Mensuration Unit, Kumasi, Ghana

6. University of York, Department of Environment and Geography, York, UK

7. Forestry Development Authority of the Government of Liberia (FDA), Monrovia, Liberia

8. Wildlife Conservation Society, DR Congo Programme, Kinshasa, Democratic Republic of Congo

9. Centre de Formation et de Recherche en Conservation Forestiere (CEFRECOF), Epulu, Democratic Republic of Congo

10. Université de Kisangani, Faculté de Gestion de Ressources Naturelles Renouvelables, Kisangani, Democratic Republic of Congo

11. University of Plymouth, School of Geography, Earth and Environmental Sciences, Plymouth, UK

12. Salonga National Park, Kinshasa, Democratic Republic of Congo

13. World Wide Fund for Nature, Gland, Switzerland

14. Norwegian University of Life Sciences, Faculty of Environmental Sciences and Natural Resource Management, Ås, Norway

15. Mbarara University of Science and Technology (MUST), The Institute of Tropical Forest Conservation (ITFC) , Mbarara, Uganda

16. Center for International Forestry Research (CIFOR), Bogor, Indonesia

17. University of Yaounde I, Plant Systematic and Ecology Laboratory, Higher Teachers' Training College, Yaounde, Cameroon

18. Manchester Metropolitan University, Department of Natural Sciences, Manchester, UK

19. University of British Columbia, Faculty of Forestry, Vancouver, Canada

20. Biodiversity International, Yaounde, Cameroon

21. University of Toronto, Faculty of Forestry, Toronto, Canada

22. Ministry of Forests, Seas, Environment and Climate, Libreville, Gabon

23. Institut de Recherche en Ecologie Tropicale, Libreville, Gabon

24. University of Stirling, Biological and Environmental Sciences, Stirling, UK

25. Forestry Research Institute of Ghana (FORIG), Kumasi, Ghana

26. Université Officielle de Bukavu, Bukavu, Democratic Republic of Congo

27. Centre for Ecology and Hydrology, Penicuik, UK

28. Ministère des Eaux, Forêts, Chasse et Pêche (MEFCP), Bangui, Central African Republic

29. Institut Centrafricain de Recherche Agronomique (ICRA), Bangui, Central African Republic

30. Centre de coopération International en Recherche Agronomique pour le Développement (CIRAD), Forêts et Sociétés (F&S), Montpellier, France

31. Université de Montpellier, Forêts et Sociétés (F&S), Montpellier, France

32. Université Marien Ngouabi, Faculté des Sciences et Techniques, Laboratoire de Botanique et Ecologie, Brazzaville, Republic of Congo

33. Ghent University, Isotope Bioscience Laboratory-ISOFYS, Gent, Belgium

34. Wildlife Conservation Society, Congo Programme, Brazzaville, Republic of Congo

35. Resources and Synergies Development (R&SD), Singapore, Singapore

36. Rougier-Gabon, Libreville, Gabon

37. University of Buea, Faculty of Science, Department of Botany and Plant Physiology, Buea, Cameroon

3

38. Duke University, Nicholas School of the Environment, Durham, NC, USA

39. University of Edinburgh, School of GeoSciences, Edinburgh, UK

40. Grantham Research Institute on Climate Change and the Environment, London, UK, London, UK

41. National Park Service, Inventory & Monitoring Program, Fredericksburg, VA, USA

42. Smithsonian Institution, Washington, DC, USA

43. University of Cambridge, Department of Plant Sciences, Cambridge, UK

44. University of Liège, Forest Resources Management, Gembloux Agro-Bio Tech, Liège, Belgium

45. University of Birmingham, School of Geography, Earth and Environmental Sciences, Birmingham, UK

46. University of Exeter, Geography, College of Life and Environmental Sciences, Exeter, UK

47. The Gola Rainforest National Park, Kenema, Sierra Leone

48. National Herbarium, Yaounde, Cameroon

49. Smithsonian Tropical Research Institute, Forest Global Earth Observatory (ForestGEO), Washington, DC, USA

50. Kunming Institute of Botany, Kunming, China

51. Royal Botanic Garden Edinburgh, Edinburgh, UK

52. Lukuru Wildlife Research Foundation, Kinshasa, Democratic Republic of Congo

53. Yale Peabody Museum of Natural History, Division of Vertebrate Zoology, New Haven, CT, USA

54. Muséum National d'Histoire Naturel, Département Hommes, natures, sociétés, Paris, France

55. Université Marien Ngouabi, École Normale Supérieure (ENS), Département des Sciences et Vie de la Terre, Laboratoire de Géomatique et d'Ecologie Tropicale Appliquée, Brazzaville, Republic of Congo

102   56. University of Bristol, School of Biological Sciences, Bristol, UK

103   57. Ghent University, Department of Environment, Computational & Applied Vegetation

104   Ecology (Cavelab), Ghent, Belgium

105   58. Tropical Ecology, Assessment and Monitoring (TEAM) Network, Arlington, VA, USA

106   59. University of Hong Kong, Department of Earth Sciences, Hong Kong, Hong Kong SAR

107   60. Wildlife Conservation Society, Uganda Programme, Kampala, Uganda

108   61. A Rocha International, Cambridge, UK

109   62. The Royal Society for the Protection of Birds, Centre of Conservation Science, Sandy, UK

110   63. Université de Kisangani, Faculté des Sciences, Laboratoire d'écologie et aménagement

111   forestier, Kisangani, Democratic Republic of Congo

112   64. Royal Botanic Gardens, Kew, UK

113   65. University of Oxford, Environmental Change Institute, School of Geography and the

114   Environment, Oxford, UK

115   66. University of the Sunshine Coast, Tropical Forests and People Research Centre, Sippy

116   Downs, Australia

117   67. Flamingo Land Ltd, Kirby Misperton, UK

118   68. Fleming College, Peterborough, Canada

119   69. Udzungwa Ecological Monitoring Centre, Mang'ula, Tanzania

120   70. Commission of Central African Forests (COMIFAC), Yaounde, Cameroon

121   71. Agence Nationale des Parcs Nationaux, Libreville, Gabon

122   72. Sokoine University of Agriculture, Morogoro, Tanzania

123   73. University of Abeokuta, Abeokuta, Nigeria

124   74. University of Southampton, School of Biological Sciences, Southampton, UK

125   75. University of Cambridge, Department of Zoology, Conservation Science Group, Cambridge,

126   UK

127   76. University of Lincoln, School of Life Sciences, Lincoln, UK

128   77. Bureau Waardenburg, Culemborg, The Netherlands

129   78. University of Florence, Department of Biology, Florence, Italy

130   79. MUSE - Museo delle Scienze, Tropical Biodiversity Section , Trento, Italy

131   80. University of Aberdeen, Department of Plant & Soil Science, School of Biological Sciences,
132   Aberdeen, UK

133   81. UK Research & Innovation, Innovate UK, London, UK

134   82. National University of Singapore, Department of Geography, Singapore, Singapore

135   83. Washington State University, Biology Department, Vancouver, WA, USA

136   84. Ministère de l'Environnement et Développement Durable, Kinshasa, Democratic Republic of
137   Congo

138   85. Université de Mbujimayi, Faculté des Sciences Appliquées, Mbujimayi, Democratic Republic
139   of Congo

140   86. Yale University, Yale School of Forestry & Environmental Studies, New Haven, CT, USA

141   87. Wildlife Conservation Society, New York, NY, USA

142   88. University of Nottingham, School of Geography, Nottingham, UK

143   89. Florida International University, International Center for Tropical Botany, Department of
144   Biological Sciences, Florida, FL, USA

145   90. Université Libre de Bruxelles, Faculté des Sciences, Service d'Évolution Biologique et
146   écologie, Brussels, Belgium

147   91. University of Bangor, School of Natural Sciences, Bangor, UK

148   92. Sommersbergseestrasse, Bad Aussee, Austria

149   93. University of Liberia, W.R.T College of Agriculture and Forestry, Monrovia, Liberia

150

151

Summary

Structurally intact tropical forests sequestered ~50% of global terrestrial carbon uptake over the 1990s and early 2000s, removing ~15% of anthropogenic CO_2 emissions[1-3]. Climate-driven vegetation models typically predict that this tropical forest 'carbon sink' will continue for decades[4,5]. Here, we assess trends in the carbon sink using 244 structurally intact African tropical forests spanning 11 countries, we compare them with 321 published plots from Amazonia and investigate the underlying drivers of the trends. The carbon sink in live aboveground biomass in intact African tropical forests has been stable for the three decades to 2015, at 0.66 Mg C ha^{-1} yr^{-1} (95% CI:0.53-0.79), in contrast to the long-term decline in Amazonian forests[6]. Thus, the carbon sink responses of Earth's two largest expanses of tropical forest have diverged. The difference is largely driven by carbon losses from tree mortality, with no detectable multi-decadal trend in Africa and a long-term increase in Amazonia. Both continents show increasing tree growth, consistent with the expected net effect of rising atmospheric CO_2 and air temperature[7-9]. Despite the past stability of the African carbon sink, our data suggest a post-2010 increase in carbon losses, delayed compared to Amazonia, indicating asynchronous carbon sink saturation on the two continents. A statistical model including CO_2, temperature, drought and forest dynamics accounts for the observed trends and indicates a long-term future decline in the African sink, while the Amazonian sink continues to rapidly weaken. Overall, the uptake of carbon into Earth's intact tropical forests peaked in the 1990s. Given that the global terrestrial carbon sink is increasing in size, observations indicating greater recent carbon uptake into the Northern hemisphere landmass[10] reinforce our conclusion that the intact tropical forest carbon sink has already saturated. This tropical forest sink saturation and ongoing decline has consequences for policies to stabilise Earth's climate.

7

Main text

178

179   Tropical forests account for approximately one-third of Earth's terrestrial Gross Primary Productivity

180   and one-half of Earth's carbon stored in terrestrial vegetation[11]. Thus, small biome-wide changes in

181   tree growth and mortality can have global impacts, either buffering or exacerbating the increase in

182   atmospheric CO_2. Models[2,4,5,7,12], ground-based observations[13-15], airborne atmospheric CO_2

183   measurements[3,16], inferences from remotely sensed data[17], and synthetic approaches[3,8,18] each suggest

184   that, after accounting for land-use change, remaining structurally intact tropical forests (i.e. not

185   impacted by direct anthropogenic impacts such as logging) are increasing in carbon stocks. This

186   structurally intact tropical forest carbon sink is estimated at ~1.2 Pg C yr^{-1} over 1990-2007 using

187   scaled inventory plot measurements[1]. Yet, despite its policy relevance, changes in this key carbon

188   sink remain highly uncertain[19,20].

189

190   Globally the terrestrial carbon sink is increasing[2,7,8,21]. Between 1990 and 2017 the land surface

191   sequestered ~30% of all anthropogenic carbon dioxide emissions[1,21]. Rising CO_2 concentrations are

192   thought to have boosted photosynthesis more than rising air temperatures have enhanced respiration,

193   resulting in an increasing global terrestrial carbon sink[2,4,7,8,21]. Yet, for Amazonia, recent results from

194   repeated censuses of intact forest inventory plots show a progressive two-decade decline in sink

195   strength primarily due to an increase of carbon losses from tree mortality[6]. It is unclear if this simply

196   reflects region-specific drought impacts[22,23], or potentially chronic pan-tropical impacts of either

197   heat-related tree mortality[24,25], or internal forest dynamics resulting from past increases in carbon

198   gains leaving the system[26]. A more recent deceleration of the rate of increase in carbon gains from

199   tree growth is also contributing to the declining Amazon sink[6]. Again, it is not known if this is a

200   result of either pan-tropical CO_2 fertilisation saturation, or rising air temperatures, or is merely a

201   regional drought impact. To address these uncertainties, we (i) analyze an unprecedented long-term

inventory dataset from Africa, (ii) pool the new African and existing Amazonian records to investigate the putative environmental drivers of changes in the tropical forest carbon sink, and (iii) project its likely future evolution.

We collected, compiled and analysed data from structurally intact old-growth forests from the African Tropical Rainforest Observation Network[27] (217 plots) and other sources (27 plots) spanning the period 1968 to 2015 (Extended Data Figure 1; Supplementary Table 1). In each plot (mean size, 1.1 ha), all trees ≥100 mm in stem diameter were identified, mapped and measured at least twice using standardised methods (135,625 trees monitored). Live biomass carbon stocks were estimated for each census date, with carbon gains and losses calculated for each interval (Extended Data Figure 2).

Continental Carbon Sink Trends

We detect no long-term trend in the per unit area African tropical forest carbon sink over three decades to 2015 (Figure 1). The aboveground live biomass sink averaged 0.66 Mg C ha^{-1} yr^{-1} (95% CI: 0.53-0.79; n=244) and was significantly greater than zero for every year since 1990 (Figure 1). While very similar to past reports (0.63 Mg C ha^{-1} yr^{-1})[13], this first estimate of the temporal trend in Africa contrasts with the declining Amazonian trend[6] (Figure 1). A linear mixed effect model shows a significant difference in the slopes of the sink trends for the two continents over the common time window (pooled data from both continents, common time window, 1983-2011.5; p=0.017). Thus, the per unit area sink strength of the two largest expanses of tropical forest on Earth diverged in the 1990s and 2000s.

The proximal cause of the divergent sink patterns is a significant increase in carbon losses (from tree mortality, i.e. the loss of carbon from the live biomass pool) in Amazonian forests, with no

227 detectable trend over three decades in African forests (Figure 1). A linear mixed effects model using

228 pooled data shows a significant difference in slopes of carbon losses between the two continents over

229 the common 1983-2011.5 time window (p=0.027). Long-term trends in carbon gains (from tree

230 growth and newly recruited trees) on both continents show significant increases (Figure 1), and we

231 could detect no difference in slopes between the continents (p=0.348; carbon gains from tree growth

232 alone also show no continental difference in long-term trends, p=0.322). However, an assessment of

233 how underlying environmental drivers affect carbon gains and losses is needed to understand the

234 ultimate causes of the divergent sink patterns.

235

236 **Understanding the Carbon Sink Trends**

237 We first investigate environmental drivers exhibiting long-term change that impact theory-driven

238 models of photosynthesis and respiration: atmospheric CO_2 concentration, surface air temperature,

239 and water availability. A linear mixed effects model of carbon gains, with censuses nested within

240 plots, and pooling the new African and published Amazonian data, shows a significant positive

241 relationship with CO_2, and significant negative relationships with mean annual temperature (MAT)

242 and drought (measured as the Maximum Climatological Water Deficit, MCWD[14]; Figure 2;

243 Extended Data Table 1). These results are consistent with a positive CO_2 fertilisation effect, and

244 negative effects of higher temperatures and drought on tree growth, consistent with temperature-

245 dependent increases in autotrophic respiration, and temperature- and drought-dependent reductions

246 in carbon assimilation. By contrast, the equivalent model for carbon losses (i.e. tree mortality) shows

247 no significant relationships with CO_2, MAT or MCWD (Figure 2; Extended Data Table 1).

248

249 We further investigate the responses of carbon gains and losses (for which the above analysis has no

250 explanatory power) by expanding our potential explanatory variables to additionally include the

251 change in environmental conditions (CO_2-change, MAT-change, MCWD-change, see Extended Data

10

252 Figure 3 for calculation details), and two attributes of forests that may influence their response to the

253 same environmental change: plot mean wood density (which in old-growth forests correlates with

254 below-ground resource availability[28,29]), and the plot carbon residence time (which measures how

255 long fixed carbon remains in the system, hence dictates when past increases in carbon gains leave the

256 system as elevated carbon losses[30]).

257

258 The minimum adequate carbon gain model using our expanded explanatory variables (best ranked

259 model using multimodel inference) has a positive relationship with CO_2-change, and negative

260 relationships with MAT, MAT-change, MCWD, and wood density (Table 2; model-average results

261 are similar, see Methods and Supplementary Tables 2-4). The retention of both MAT and MAT-

262 change suggests that higher temperatures correspond to lower tree growth, and that trees only

263 partially acclimate to recently rising temperatures, which further reduces growth, consistent with

264 warming experiments[31] and observations[9]. The inclusion of higher wood density, and it being related

265 to lower carbon gains (Extended Data Figure 4), alongside no temporal trends in wood density

266 (Extended Data Figure 5), suggests that old-growth forests with denser-wooded tree communities

267 typically have fewer available below-ground resources, or such patterns may also emerge from

268 disturbance regimes lacking large-scale exogenous events, consistent with prior studies[26,28,32].

269

270 The minimum adequate carbon gain model using our expanded explanatory variables also highlights

271 continental differences. Between 2000 and 2015 African forest carbon gains increased by 3.1%

272 compared with a 0.1% decline in Amazonia over the same interval (Table 2). In Africa, from 2000 to

273 2015, the increase was composed of a 3.7% increase from CO_2-change, partially offset by increasing

274 droughts depleting gains by 0.5%, and only a slight decline in gains of 0.1% resulting from

275 temperature increases (Table 2), because the rate of temperature change (MAT-change) decelerated

276 over this time window (Extended Data Figure 5). For Amazonia, the same 3.7% increase due to CO_2-

277 change was seen, while increasing droughts—and these forests' greater sensitivity to drought—

278 reduced gains by 2.7% (five times the impact in Africa), and temperature increases at the same rate

279 as in the past (i.e. MAT-change is zero) further reduced gains by 1.1% (ten times the impact in

280 Africa), leaving a net change in gains slightly below zero (Table 2). Thus, the recent stalling of

281 carbon gain increases in Amazonia[6] is a response to drought and temperature and not due to an

282 unexpected saturation of CO_2 fertilisation. Overall, the larger modelled increase in gains in Africa

283 relative to Amazonia appear to be driven by slower warming, fewer or less extreme droughts, lower

284 forest sensitivity to droughts, and overall lower temperatures (African forests are on average ~1.1°C

285 cooler than Amazonian forests, as they typically grow at ~200 m higher elevation). Other continental

286 differences may also be influencing the results, including higher nitrogen deposition in African

287 tropical forests due to the seasonal burning of nearby savannas[33] and biogeographic history resulting

288 in differing contemporary species pools and resulting functional attributes[34,35].

289

290 The minimum adequate carbon loss model using our expanded explanatory variables shows higher

291 losses with CO_2-change and MAT-change, and lower losses with MCWD and the carbon residence

292 time (CRT; Table 2). Thus, changes in carbon losses appear to be largely a function of carbon gains.

293 First, the greater losses in forests with shorter CRT conform to a 'high-gain high-loss' forest

294 dynamics pattern[26]. Second, wetter plots have a longer growing season and so have higher gains and

295 correspondingly higher losses, explaining the negative relationship with MCWD. Third, as

296 increasing CO_2 levels result in additional carbon gains, after some time these additional past gains

297 leave the system resulting in greater carbon losses, explaining the positive relationship with CO_2-

298 change. Finally, in addition to these relationships with carbon gains, the inclusion of MAT-change

299 (p<0.001) indicates heat- or vapour pressure deficit-induced tree mortality[24]. Overall, our results

300 imply that chronic long-term environmental change factors, temperature and CO_2, rather than simply

301 the direct effects of drought, underlie longer-term trends in tropical forest tree mortality, although

302 other changes such as rising liana infestation rates seen in Amazonia[36,37] cannot be excluded.

303

304 The minimum adequate carbon loss model using our expanded explanatory variables replicates the

305 continental trends (Figure 3). The overall lower loss rates in Africa reflect their longer CRT (69 yrs,

306 95% CI, 66-72), compared with Amazonian forests (56 yrs, 95% CI, 54-59) while over the 2000-

307 2015 window the much smaller increase in loss rates in Africa compared to Amazonia results from a

308 slower increase in warming and a stable CRT in Africa compared to continued warming at previous

309 rates and a shortening CRT in Amazonian forests (Extended Data Figure 5). Furthermore, given that

310 losses appear to lag behind gains they should relate to the long-term CRT of plots. This is what we

311 find: the longer the CRT the smaller the increase in carbon losses, with no increase in losses for plots

312 with CRT ≥77 years (Extended Data Figure 6). Consequently, due to the typically longer residence

313 times of African forests, increasing losses in Africa ought to appear 10-15 years after the increase in

314 Amazon losses began (*c*.1995). Strikingly, in Africa the most intensely monitored plots suggest that

315 losses began increasing from *c*.2010 (Extended Data Figure 7), and plots with shorter CRT are

316 driving the increase (Extended Data Figure 8). Thus, a mortality-dominated African carbon sink

317 decline appears to have begun very recently.

318

319 **Future of the Tropical Forest Carbon Sink**

320 Our carbon gain and loss models (Table 2) can be used to make a tentative estimate of the future size

321 of the per unit area intact forest carbon sink (Figure 3). Extrapolations of the changes in the predictor

322 variables from 1983-2015 forward to 2040 (Extended Data Figure 5) show declines in the sink on

323 both continents (Figure 3). By 2030 the carbon sink in aboveground live biomass in intact African

324 tropical forest is predicted to decline by 14% from the measured 2010-15 mean, to 0.57 Mg C ha^{-1} yr^{-1}

325 ^{1} (2σ range, 0.16-0.96; Figure 3). The Amazon sink continues to decline, reaching zero in 2035 (2σ

13

326 range, 2011-2089; Figure 3). Our estimated sink strength on both continents in the 2020s and 2030s

327 is sensitive to future CO_2 emissions pathways (CO_2-change)[38], resulting temperature increase (MAT,

328 MAT-change) and hydrological changes (MCWD), plus changes in forest dynamics (CRT), but the

329 sink is always lower than levels seen in the 2000s (see Methods and Supplementary Table 5). Thus,

330 the carbon sink strength of the world's two most extensive tropical forests have now saturated, albeit

331 asynchronously.

332

333 **Scaling Results to the Pan-tropics**

334 Scaling our estimated mean sink strength by forest area for each continent signifies that Earth

335 recently passed the point of peak carbon sequestration into intact tropical forests (Table 1). The

336 continental sink in Amazonia peaked in the 1990s, followed by a decline, driven by sink strength

337 peaking in the 1990s and a continued decline in forest area (Table 1). In Africa the per unit area sink

338 strength peaked later in the 2000-2010 period, but the continental African sink peaked in the 1990s,

339 due to the decline in forest area in the 2000s outpacing the small per unit area increase in sink

340 strength. Including the modest uptake in the much smaller area of intact Asian tropical forest

341 indicates that total pan-tropical carbon uptake peaked in the 1990s (Table 1). From peak pan-tropical

342 intact forest uptake of 1.26 Pg C yr^{-1} in the 1990s, we project a continued decline reaching just 0.29

343 Pg C yr^{-1} in the 2030s (multi-decade decline of ~0.24 Pg C yr^{-1} decade^{-1}), driven by (i) reduced mean

344 pan-tropical sink strength decline of 0.1 Mg C ha^{-1} yr^{-1} decade^{-1} and (ii) ongoing forest area losses of

345 ~13.5 million ha yr^{-1} (see Extended Data Table 2 for forest area details). Critically, climate-driven

346 vegetation model simulations have not predicted that peak net carbon uptake into intact tropical

347 forests has already been passed[2,4,5].

348

14

Discussion

Our method of scaling to arrive at a pan-tropical sink estimate – in common with other studies using similar datasets[1,6,13] – is limited. Yet, pervasive net carbon uptake is expected given that we find a strong and ongoing CO_2 fertilisation effect. Using our CO_2 response in Table 2, we find an increase in aboveground carbon stocks of 10.8±3.7 Mg C ha^{-1} 100 ppm^{-1} CO_2, or 6.5±2.2% (±SE; using an area-weighted pan-tropical mean aboveground C stock of 165 Mg C ha^{-1}), comparable to the 5.0±1.2% increase in tropical forest C stocks 100 ppm^{-1} CO_2 derived from a recent synthesis of CO_2 fertilisation experiments, despite a lack of data from mature tropical forests[39]. Our result is within the range of climate-driven vegetation models[2,7], although it is greater than a number of recently-published models that include potential nutrient constraints, reported as 5.9±4.7 Mg C ha^{-1} 100 ppm^{-1} CO_2 (Ref.[40]). We find that the CO_2 fertilisation uptake is currently only partially offset by the negative impacts of similarly widespread rising air temperatures (-2.0±0.4 Mg C ha^{-1} °C^{-1}, from Table 2), consistent with models[7], limited experiments[31] and independent observations[9], plus negative responses to drought[41,42]. Long-term and extensive increases in satellite-derived greenness in tropical regions not experiencing major changes in land-use management[17,43], particularly in central Africa in the past decade[44], indicate increases in tropical forest net primary productivity, providing further evidence that the sink is a widespread phenomenon[44].

Nonetheless, our analyses show that this pervasive tropical forest sink in live biomass is in long-term decline, first saturating in Amazonia, and more recently followed by African forests, explaining the prior Africa-Amazon carbon sink divergence as part of a longer-term pattern of asynchronous saturation and decline. From an atmospheric perspective the full impacts of the contribution to the saturation of the sink from slowing carbon gains are experienced immediately, but the contribution from rising carbon losses is delayed because dead trees do not decompose instantaneously. Decomposition of this dead tree mass is ~50% in 4 yrs, and ~85% in 10 yrs, thus rising carbon losses

15

374 result in delayed carbon additions to the atmosphere[45]. Hence, from an atmospheric perspective the

375 intact tropical forest biomass carbon sink likely peaked a few years later than our plot data indicate

376 and the full impacts are not yet realised. The pan-tropical carbon sink in live biomass reduced by

377 0.27 Pg C yr^{-1} between the 1990s and 2000s (Table 1), but accounting for dead wood

378 decomposition[45] shows a smaller 0.17 Pg C yr^{-1} reduction from an atmospheric perspective (see

379 Methods).

380

381 Given that the global terrestrial carbon sink is increasing, a weakening intact tropical forest sink

382 implies that the extra-tropical carbon sink has increased over the past two decades. Independent

383 observations of inter-hemispheric atmospheric CO_2 concentration indicates that carbon uptake into

384 the Northern hemisphere landmass has increased at a greater rate than the global terrestrial carbon

385 sink since the 1990s, with a further disproportionate increase in the 2000s[10]. The inter-hemispheric

386 analysis suggests a weakening of the tropical forest sink by ~0.2 Pg C yr^{-1} between the 1990s and

387 2000s[10], which is similar to the 0.17 Pg C yr^{-1} weakening over the same time period that we find.

388 This reinforces our conclusion that the intact tropical forest carbon sink has already saturated.

389

390 In summary, our results indicate that while intact tropical forests remain major stores of carbon and

391 are key centres of biodiversity[11], their ability to sequester additional carbon is waning. In the 1990s

392 intact forests removed 17% of anthropogenic CO_2 emissions. This has declined to 6% in the 2010s,

393 because the pan-tropical weighted average per unit area sink strength declined by 33%, forest area

394 decreased by 19%, and CO_2 emissions increased by 46%. Although tropical forests are more

395 immediately threatened by deforestation[46] and degradation[47], and the future carbon balance will also

396 depend on secondary forest dynamics[48] and forest restoration plans[49], our analyses show that they are

397 also impacted by atmospheric chemistry and climatic changes. Given that the intact tropical forest

398 carbon sink is set to end sooner than even the most pessimistic climate-driven vegetation models

399 predict[4,5], our analyses suggest that climate change impacts in the tropics may become more severe

400 than predicted. Furthermore, the carbon balance of intact tropical forests will only stabilise once CO_2

401 concentrations and the climate stabilises.

402

403 Continued on-the-ground monitoring of the world's remaining intact tropical forests will be required

404 to test our prediction that the intact tropical forest carbon sink will continue to decline. Such direct

405 ground-based measurements also provide a constraint on estimating the size and location of the

406 terrestrial carbon sink. In addition, our conclusion that tree mortality and internal forest dynamics are

407 important controls on the future of the tropical forest carbon sink, may assist in improving the

408 vegetation components of future Earth System Models[50] and contribute to reducing terrestrial carbon

409 cycle feedback uncertainty[19,20]. Our findings also have policy implications. At the country-level:

410 given intact tropical forests are a carbon sink, but the size is changing, national greenhouse gas

411 reporting will require careful forest monitoring. At the international-level: given tropical forests are

412 likely to sequester less carbon in the future than Earth System Models predict, an earlier date to reach

413 net zero anthropogenic greenhouse gas emissions will be required to meet any given commitment to

414 limit the global heating of Earth.

415

416 **References**

417

418 1   Pan, Y. *et al.* A Large and Persistent Carbon Sink in the World's Forests. *Science* **333**, 988-

419   993, doi:10.1126/science.1201609 (2011).

420 2   Sitch, S. *et al.* Recent trends and drivers of regional sources and sinks of carbon dioxide.

421   *Biogeosciences* **12**, 653-679, doi:10.5194/bg-12-653-2015 (2015).

422 3   Gaubert, B. *et al.* Global atmospheric CO_2 inverse models converging on neutral tropical land

423   exchange, but disagreeing on fossil fuel and atmospheric growth rate. *Biogeosciences* **16**,

424   117-134, doi:10.5194/bg-16-117-2019 (2019).

425 4   Huntingford, C. *et al.* Simulated resilience of tropical rainforests to CO_2-induced climate

426   change. *Nature Geoscience* **6**, 268-273, doi:10.1038/ngeo1741 (2013).

427 5   Mercado, L. M. *et al.* Large sensitivity in land carbon storage due to geographical and

428   temporal variation in the thermal response of photosynthetic capacity. *New Phytologist* **218**,

429   1462-1477, doi:doi:10.1111/nph.15100 (2018).

430 6   Brienen, R. J. W. *et al.* Long-term decline of the Amazon carbon sink. *Nature* **519**, 344-348,

431   doi:10.1038/nature14283 (2015).

432 7   Piao, S. *et al.* Evaluation of terrestrial carbon cycle models for their response to climate

433   variability and to CO_2 trends. *Global Change Biology* **19**, 2117-2132, doi:10.1111/gcb.12187

434   (2013).

435 8   Schimel, D., Stephens, B. B. & Fisher, J. B. Effect of increasing CO_2 on the terrestrial carbon

436   cycle. *Proceedings of the National Academy of Sciences* **112**, 436-441,

437   doi:10.1073/pnas.1407302112 (2015).

438 9   Anderegg, W. R. L. *et al.* Tropical nighttime warming as a dominant driver of variability in

439   the terrestrial carbon sink. *Proceedings of the National Academy of Sciences* **112**, 15591-

440   15596, doi:10.1073/pnas.1521479112 (2015).

441 10   Ciais, P. *et al.* Five decades of northern land carbon uptake revealed by the interhemispheric

442   CO_2 gradient. *Nature*, doi:10.1038/s41586-019-1078-6 (2019).

443 11   Lewis, S. L., Edwards, D. P. & Galbraith, D. Increasing human dominance of tropical forests.

444   *Science* **349**, 827-832, doi:10.1126/science.aaa9932 (2015).

445 12   Pugh, T. A. M. *et al.* Role of forest regrowth in global carbon sink dynamics. *Proceedings of*

446   *the National Academy of Sciences* **116**, 4382-4387, doi:10.1073/pnas.1810512116 (2019).

447 13   Lewis, S. L. *et al.* Increasing carbon storage in intact African tropical forests. *Nature* **457**,

448   1003-1006, doi:10.1038/nature07771 (2009).

449   14   Phillips, O. L. *et al.* Drought sensitivity of the Amazon rainforest. *Science* **323**, 1344-1347,

450   doi:10.1126/science.1164033 (2009).

451   15   Qie, L. *et al.* Long-term carbon sink in Borneo's forests halted by drought and vulnerable to

452   edge effects. *Nature Communications* **8**, 1966, doi:10.1038/s41467-017-01997-0 (2017).

453   16   Gatti, L. V. *et al.* Drought sensitivity of Amazonian carbon balance revealed by atmospheric

454   measurements. *Nature* **506**, 76-80, doi:10.1038/nature12957 (2014).

455   17   Nemani, R. R. *et al.* Climate-driven increases in global terrestrial net primary production

456   from 1982 to 1999. *Science* **300**, 1560-1563 (2003).

457   18   Keenan, T. F. *et al.* Recent pause in the growth rate of atmospheric CO_2 due to enhanced

458   terrestrial carbon uptake. *Nature Communications* **7**, 13428, doi:10.1038/ncomms13428

459   (2016).

460   19   Booth, B. B. B. *et al.* High sensitivity of future global warming to land carbon cycle

461   processes. *Environmental Research Letters* **7**, 024002 (2012).

462   20   Lombardozzi, D. L., Bonan, G. B., Smith, N. G., Dukes, J. S. & Fisher, R. A. Temperature

463   acclimation of photosynthesis and respiration: A key uncertainty in the carbon cycle-climate

464   feedback. *Geophysical Research Letters* **42**, 8624-8631, doi:doi:10.1002/2015GL065934

465   (2015).

466   21   Le Quéré, C. *et al.* Global Carbon Budget 2018. *Earth Syst. Sci. Data* **10**, 2141-2194,

467   doi:10.5194/essd-10-2141-2018 (2018).

468   22   Lewis, S. L., Brando, P. M., Phillips, O. L., van der Heijden, G. M. F. & Nepstad, D. The

469   2010 Amazon Drought. *Science* **331**, 554 (2011).

470   23   Feldpausch, T. R. *et al.* Amazon forest response to repeated droughts. *Global

471   Biogeochemical Cycles* **30**, 964-982, doi:doi:10.1002/2015GB005133 (2016).

472   24   McDowell, N. *et al.* Drivers and mechanisms of tree mortality in moist tropical forests. *New

473   Phytologist* **219**, 851-869, doi:doi:10.1111/nph.15027 (2018).

474   25   Aleixo, I. *et al.* Amazonian rainforest tree mortality driven by climate and functional traits.

475   *Nature Climate Change* **9**, 384-388, doi:10.1038/s41558-019-0458-0 (2019).

476   26   Lewis, S. L. *et al.* Concerted changes in tropical forest structure and dynamics: evidence from

477   50 South American long-term plots. *Philosophical Transactions of the Royal Society of*

478   *London Series B-Biological Sciences* **359**, 421-436 (2004).

479   27   Lewis, S. L. *et al.* Above-ground biomass and structure of 260 African tropical forests.

480   *Philosophical Transactions of the Royal Society B: Biological Sciences* **368**, 20120295-

481   20120295, doi:10.1098/rstb.2012.0295 (2013).

482   28   Quesada, C. A. *et al.* Basin-wide variations in Amazon forest structure and function are

483   mediated by both soils and climate. *Biogeosciences* **9**, 2203-2246, doi:10.5194/bg-9-2203-

484   2012 (2012).

485   29   Malhi, Y. *et al.* The above-ground coarse wood productivity of 104 Neotropical forest plots.

486   *Global Change Biology* **10**, 563-591 (2004).

487   30   Galbraith, D. *et al.* Residence times of woody biomass in tropical forests. *Plant Ecology &*

488   *Diversity* **6**, 139-157, doi:10.1080/17550874.2013.770578 (2013).

489   31   Reich, P. B. *et al.* Boreal and temperate trees show strong acclimation of respiration to

490   warming. *Nature* **531**, 633-636, doi:10.1038/nature17142 (2016).

491   32   ter Steege, H. *et al.* Continental-scale patterns of canopy tree composition and function across

492   Amazonia. *Nature* **443**, 444-447 (2006).

493   33   Bauters, M. *et al.* High fire-derived nitrogen deposition on central African forests.

494   *Proceedings Of The National Academy Of Sciences Of The United States Of America* **115**,

495   549-554, doi:10.1073/pnas.1714597115 (2018).

496   34   Parmentier, I. *et al.* The odd man out? Might climate explain the lower tree alpha-diversity of

497   African rain forests relative to Amazonian rain forests? *Journal of Ecology* **95**, 1058-1071

498   (2007).

499 35 Slik, J. W. F. *et al.* Phylogenetic classification of the world's tropical forests. *Proceedings of*

500 *the National Academy of Sciences* **115**, 1837-1842, doi:10.1073/pnas.1714977115 (2018).

501 36 Phillips, O. L. *et al.* Increasing dominance of large lianas in Amazonian forests. *Nature* **418**,

502 770-774 (2002).

503 37 Schnitzer, S. A. & Bongers, F. Increasing liana abundance and biomass in tropical forests:

504 emerging patterns and putative mechanisms. *Ecology Letters* **14**, 397-406,

505 doi:10.1111/j.1461-0248.2011.01590.x (2011).

506 38 Meinshausen, M. *et al.* The RCP greenhouse gas concentrations and their extensions from

507 1765 to 2300. *Climatic Change* **109**, 213-241, doi:10.1007/s10584-011-0156-z (2011).

508 39 Terrer, C. *et al.* Nitrogen and phosphorus constrain the CO_2 fertilization of global plant

509 biomass. *Nature Climate Change*, doi:10.1038/s41558-019-0545-2 (2019).

510 40 Fleischer, K. *et al.* Amazon forest response to CO_2 fertilization dependent on plant

511 phosphorus acquisition. *Nature Geoscience* **12**, 736-741, doi:10.1038/s41561-019-0404-9

512 (2019).

513 41 Jiang, Y. *et al.* Widespread increase of boreal summer dry season length over the Congo

514 rainforest. *Nature Climate Change* **9**, 617-622, doi:10.1038/s41558-019-0512-y (2019).

515 42 Gloor, M. *et al.* Recent Amazon climate as background for possible ongoing and future

516 changes of Amazon humid forests. *Global Biogeochemical Cycles* **29**, 1384-1399,

517 doi:10.1002/2014gb005080 (2015).

518 43 Kolby Smith, W. *et al.* Large divergence of satellite and Earth system model estimates of

519 global terrestrial CO_2 fertilization. *Nature Climate Change* **6**, 306, doi:10.1038/nclimate2879

520 (2015).

521 44 Chen, C. *et al.* China and India lead in greening of the world through land-use management.

522 *Nature Sustainability* **2**, 122-129, doi:10.1038/s41893-019-0220-7 (2019).

523   45   Chambers, J. Q., Higuchi, N., Schimel, J. P., Ferreira, L. V. & Melack, J. M. Decomposition

524   and carbon cycling of dead trees in tropical forests of the central Amazon. *Oecologia* **122**,

525   380-388 (2000).

526   46   Hansen, M. C. *et al.* High-Resolution Global Maps of 21st-Century Forest Cover Change.

527   *Science* **342**, 850-853, doi:10.1126/science.1244693 (2013).

528   47   Pearson, T. R. H., Brown, S., Murray, L. & Sidman, G. Greenhouse gas emissions from

529   tropical forest degradation: an underestimated source. *Carbon Balance and Management* **12**,

530   3, doi:10.1186/s13021-017-0072-2 (2017).

531   48   Schwartz, N. B., Uriarte, M., DeFries, R., Gutierrez-Velez, V. H. & Pinedo-Vasquez, M. A.

532   Land-use dynamics influence estimates of carbon sequestration potential in tropical second-

533   growth forest. *Environmental Research Letters* **12**, 074023, doi:10.1088/1748-9326/aa708b

534   (2017).

535   49   Lewis, S. L., Wheeler, C. E., Mitchard, E. T. A. & Koch, A. Regenerate natural forests to

536   store carbon. *Nature* **568**, 25-28 (2019).

537   50   Yu, K. *et al.* Pervasive decreases in living vegetation carbon turnover time across forest

538   climate zones. *Proceedings of the National Academy of Sciences*, 201821387,

539   doi:10.1073/pnas.1821387116 (2019).

540

Acknowledgements

655

Author Contributions

657   S.L.L. conceived and managed the AfriTRON forest plot recensus programme, O.L.P., T.C.H.S,

658   L.J.T.W. and Y.M. contributed to its development. W.H., S.L.L., O.L.P., B.S. & M.J.P.S. developed

659   the study. W.H., S.L.L., O.L.P., K.A.-B., H.B., A.C.-S., C.E.N.E., S.F., D.S., B.S., T.C.H.S., S.C.T.,

660   K.A.A., S.A.-B., C.A.A., T.R.B., L.F.B., F.Ba., S.K.B., F.Be., R.B., Y.E.B., P.Boe., P.Bou., T.B.,

661   E.C., G.B.C., C.J.C., M.C., J.A.C., D.C., A.K.D., G.C.D., T.d.H., M.D.K., J.-L.D., T.R.F., A.F.,

662   E.G.F., M.G., C.G., S.G.-F., J.S.H., A.C.H., D.J.H., T.B.H., M.B.N.H., A.H., S.A.I., K.J.J., T.J.,

663   E.K.Y., E.K., D.K., M.E.L., J.A.L., J.L., J.C.L., J.-R.M., Y.M., A.R.M., J.M., E.H.M., F.M.M.,

664   V.P.M., V.M., E.T.A.M., S.M., J.M.M., P.K.T.M., N.N.B., L.O., F.E., K.P., A.D.P., J.R.P., L.Q.,

665   J.R., F.R., M.D.S., H.T., J.Tal., J.Tap., D.M.T., D.W.T., B.T., J.T.M., D.T., P.M.U., G.V.D.H., H.V.,

666   J.V., L.J.T.W., S.W., H.W., J.T.W. and L.Z. contributed data (larger field contributions by S.L.L,

667   W.H., A.C.-S., B.S., H.T., A.K.D., C.E.N.E, J.M.M., K.A.-B. and S.F.). O.L.P., T.R.B., S.L.L. and

668   G.L.-G. conceived and managed forestplots.net; O.L.P., T.R.B., S.L.L., E.G., G.L.-G., G.C.P., A.L.,

669   R.J.W.B., T.R.F. and M.J.P.S. developed it. W.H., M.J.P.S., S.L.L., O.L.P., R.J.W.B., A.L., G.L.-G.,

670   A.E.-M., A.K., E.G., T.R.B., A.C.B. and G.C.P. contributed analysis tools. W.H. and S.L.L. analysed

671   the data (with important contributions from M.J.P.S.). S.L.L. and W.H. wrote the paper. All co-

672 authors read and approved the manuscript (with important insights provided by O.L.P., S.F.,

673 R.J.W.B., E.G., H.B., D.S., M.J.P.S., S.G.-F., P.B., H.V. and S.C.T).

674

675 **Main Figures**
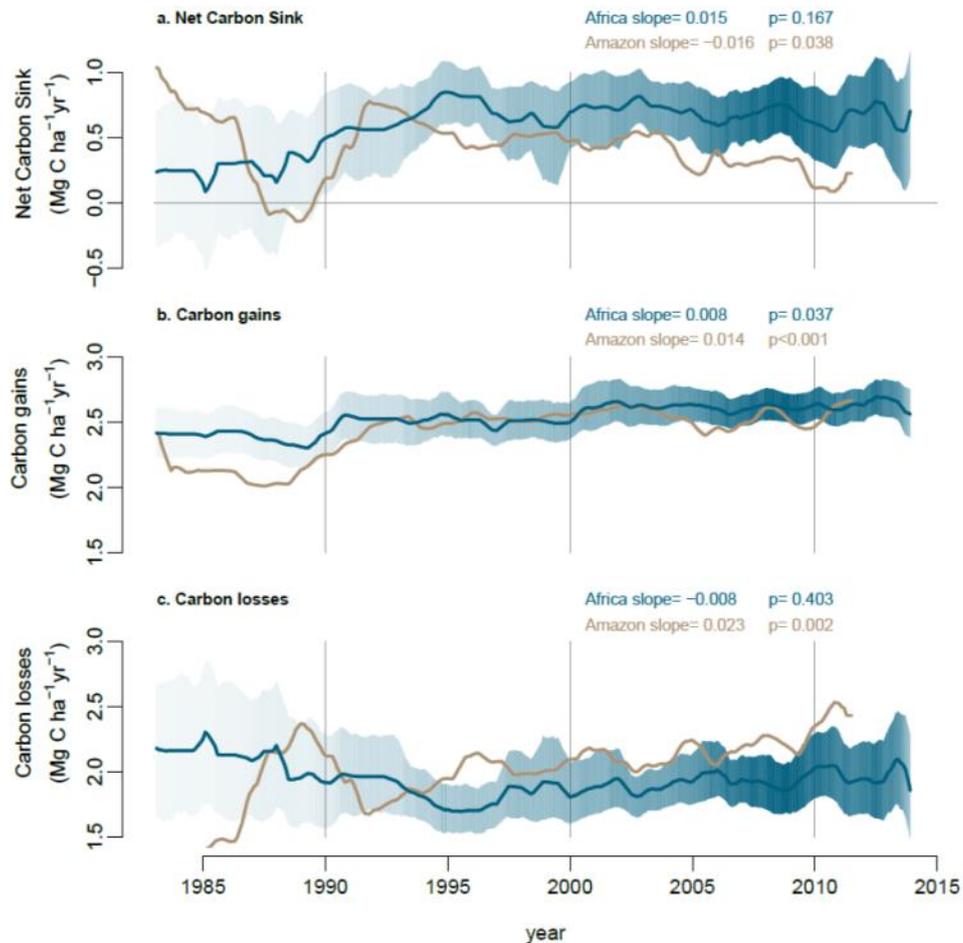
676

677 **Figure 1. Long-term carbon dynamics of structurally intact tropical forests in Africa (blue)**

678 **and Amazonia (brown).** Trends in net aboveground live biomass carbon sink (**a**), carbon gains to

679 the system from wood production (**b**), and carbon losses from the system from tree mortality (**c**),

680 measured in 244 African inventory plots (blue lines) and contrasting published[6] Amazonian

681 inventory data (brown lines; 321 plots). Shading corresponds to the 95% CI, with less transparent

682 shading indicating a greater number of plots monitored in that year (most transparent: minimum 25

683 plots monitored). The CI for the Amazonian dataset is omitted for clarity, but can be seen in Figure

684 3. Slopes and p-values are from linear mixed effects models (see Methods).

685
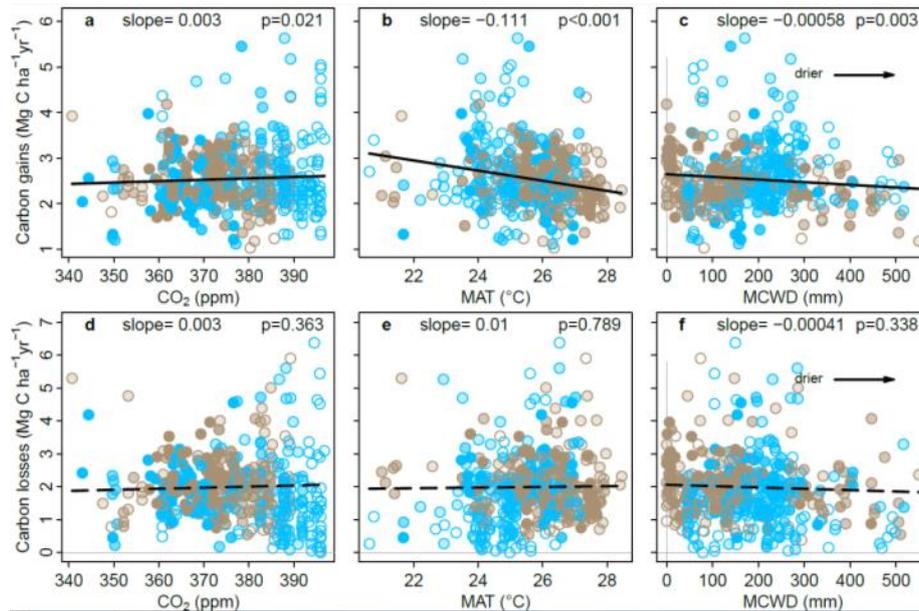
Figure 2. Potential environmental drivers of carbon gains and losses in structurally intact old-growth African and Amazonian tropical forests. Aboveground carbon gains, from woody production (**a-c**), and aboveground carbon losses, from tree mortality (**d-f**), presented as time-weighted mean values for each plot, i.e. each census within a plot is weighted by its length, against the corresponding values of atmospheric carbon dioxide concentration (CO_2), mean annual air temperature (MAT) and drought (as Maximum Climatological Water Deficit, MCWD), for African (blue) and Amazonian (brown) inventory plots. Each data point therefore represents an inventory plot, for visual clarity, and the level of transparency represents the total monitoring length, with empty circles corresponding to plots monitored for ≤ 5 years and solid circles for plots monitored for >20 years. Solid lines show significant trends, dashed lines non-significant trends calculated using linear mixed effect models with census intervals (n=1566) nested within plots (n=565), using an empirically derived weighting based on interval length and plot area, on the untransformed pooled Africa and Amazon dataset (see Methods). Slopes and p-values are from the same linear mixed effects models. Carbon loss data and models are presented untransformed for comparison with carbon gains, but transformation is needed to fit normality assumptions; linear mixed effects models on transformed carbon loss data does not change the significance of the results, nor does including all three parameters and transformed data in a model (see Extended Data Table 1).

703
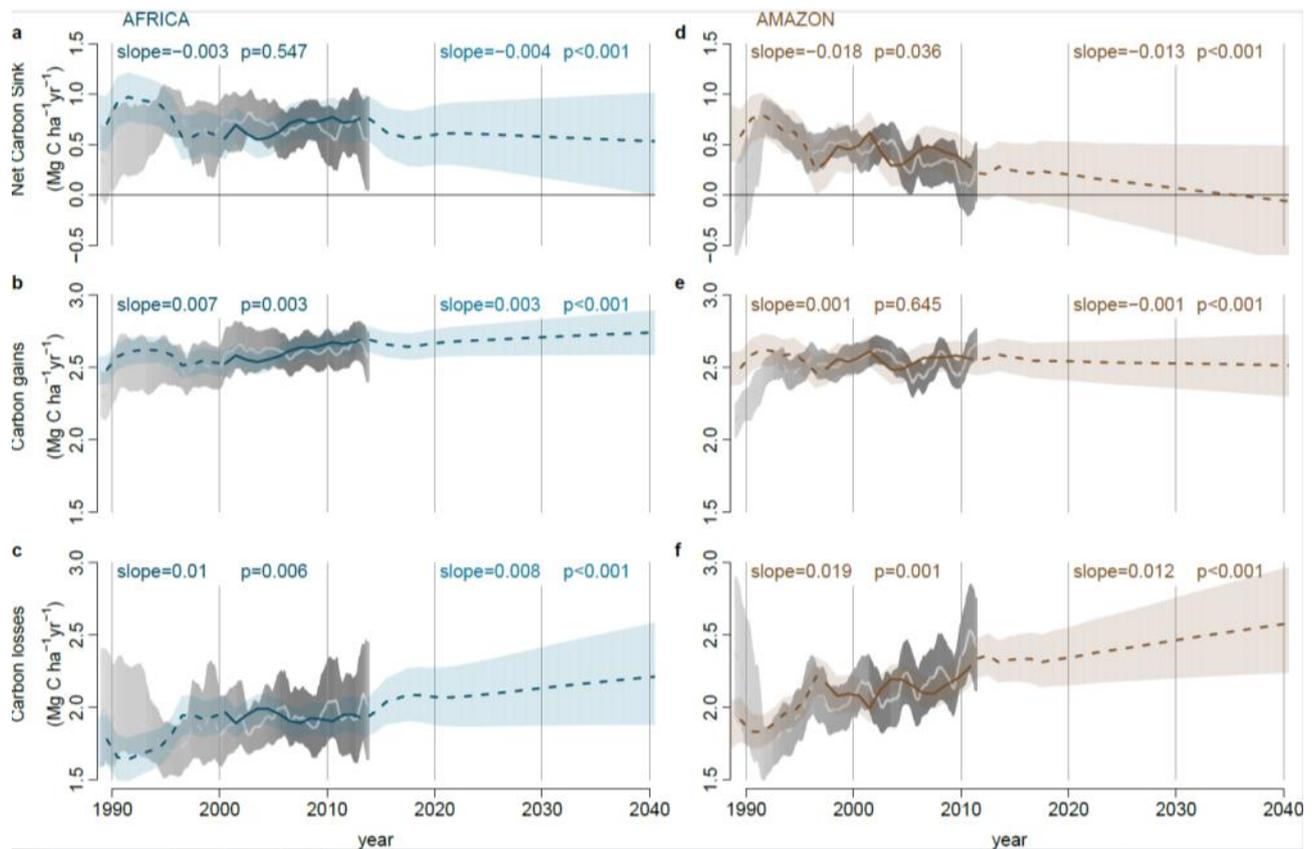
Figure 3. Modelled past and future carbon dynamics of structurally intact tropical forests in Africa and Amazonia. Predictions of net aboveground live biomass carbon sink (**a,d**), carbon gains (**b,e**), and carbon losses (**c,f**), for African (left panels) and Amazonian (right panels) plot inventory networks, based on CO_2-change, Mean Annual Temperature, Mean Annual Temperature-change, drought (as Maximum Climatological Water Deficit), plot wood density, and plot carbon residence time, using observations in Africa until 2014 and Amazonia until 2011.5, and extrapolations of prior trends to 2040. Model predictions are in blue (Africa) and brown (Amazon), with solid lines spanning the window when ≥75% of plots were monitored to show model consistency with the observed trends, and shading showing upper and lower confidence intervals accounting for uncertainties in the model (both fixed and random effects) and uncertainties in the predictor variables. Light grey lines and grey shading are the mean and 95% CI of the observations from the African and Amazonian plot networks.

30

Main Tables

Table 1. Carbon sink in intact forests in Africa, Amazonia and the pan-tropics: 1980-2015 and predictions to 2040. Mean values in bold, future predictions in italics, uncertainty in parentheses, 95% bootstrapped confidence intervals for 1980-2015, and 2σ for the predictions (2010-2040).

Period	No. plots		Per unit area aboveground live biomass C sink (Mg C ha⁻¹ yr⁻¹)			Total C sink * (Pg C yr⁻¹)		
	Af.	Am.	Africa	Amazon	Pan-tropics†	Africa	Amazon	Pan-tropics†
1980-1990	45	73	**0.33** (0.06-0.63)	**0.35** (0.06-0.59)	**0.35** (0.07-0.62)	**0.28** (0.05-0.53)	**0.49** (0.08-0.82)	**0.87** (0.16-1.52)
1990-2000	96	172	**0.67** (0.43-0.89)	**0.53** (0.42-0.65)	**0.57** (0.39-0.74)	**0.50** (0.32-0.66)	**0.68** (0.54-0.83)	**1.26** (0.88-1.63)
2000-2010	194	291	**0.70** (0.55-0.84)	**0.38** (0.26-0.48)	**0.50** (0.35-0.64)	**0.46** (0.37-0.56)	**0.45** (0.31-0.57)	**0.99** (0.70-1.25)
2010-2015	184	172	**0.66** (0.40-0.91)	**0.24** (0.00-0.47)	**0.40** (0.15-0.65)	**0.40** (0.24-0.56)	**0.27** (0.00-0.52)	**0.73** (0.25-1.18)
2010-2020 ‡	-	-	*0.63 (0.36-0.89)*	*0.23 (-0.05-0.50)*	*0.38 (0.11-0.65)*	*0.37 (0.21-0.53)*	*0.25 (-0.05-0.54)*	*0.68 (0.17-1.16)*
2020-2030 ‡	-	-	*0.59 (0.24-0.93)*	*0.12 (-0.29-0.51)*	*0.30 (-0.08-0.67)*	*0.31 (0.13-0.49)*	*0.12 (-0.29-0.52)*	*0.47 (-0.15-1.07)*
2030-2040 ‡	-	-	*0.55 (0.08-0.99)*	*0.00 (-0.54-0.49)*	*0.21 (-0.29-0.67)*	*0.26 (0.04-0.47)*	*0.00 (-0.50-0.46)*	*0.29 (-0.46-0.97)*

* Total Continental C sink is the per unit area aboveground C sink multiplied by intact forest area for 1990-2010 (from ref.[1], see Extended Data Table 2) and continent specific extrapolations to 2040. Total Continental C sink includes continent-specific estimates of trees <100 mm DBH, lianas and roots (see Methods).

† Pan-tropical aboveground live biomass C sink is the area-weighted mean of African, Amazonian and Southeast Asian sink values. Southeast Asian values were from published per unit area carbon sink data[15] (n=49 plots) for 1990-2015, with 1980-1990 assumed to be the same as 1990-2000 due very low sample sizes. Pan-tropical total C sink is the sum of African, Amazonian and Southeast Asian total continental carbon sink values. The continental sink in Southeast Asia is a modest and declining contribution to the pan-tropical sink, due to the very small area of intact forest remaining, at 0.11, 0.08, 0.07 and 0.06 Pg C yr⁻¹ in the 1980s, 1990s, 2000s and 2010s, hence uncertainty in the Southeast Asian sink cannot reverse the pan-tropical declining sink trend.

‡ Per unit area total C sink for 2010-2020, 2020-2030 and 2030-2040 was predicted using parameters from Table 2, except for the 2010-2020 sink in Africa which is the mean of the measured sink from 2010-2015 and the modelled sink from 2015-2020. For the Asian sink we assumed the parameters as for Africa, as Asian forest median CRT is 61 years, close to African median, 63 years.

Table 2. Minimum adequate models to predict carbon gains and losses in African and Amazonian tropical forests. These are the best ranked gains and loss models. Where continental values differ, those for Africa are reported first, followed by Amazonian values.

Carbon gains, Mg C ha^{-1} yr^{-1}				
Predictor variable	**Parameter value**	**Standard Error**	**t-value**	**p-value**	**2000-2015 change in gains (%) ***
(Intercept)	5.255 | 5.395	0.603 | 0.614	8.7 | 8.8	<0.001	-
CO_2-change (ppm yr^{-1}) †	0.238	0.096	2.5	0.013	3.69% | 3.71%
MAT (°C)	-0.083	0.025	-3.3	0.001	-0.67% | -1.07%
MAT-change (°C yr^{-1}) ‡	-1.243	0.233	-5.3	<0.001	0.58% | 0.00% §
MCWD (mm x1000)	-0.405 | -1.391	0.381 | 0.24	-1.1 | -5.8	0.289 | <0.001	-0.52% | -2.73%
WD (g cm^{-3})	-1.295	0.530	-2.4	0.015	0.05% | 0.00%
Carbon losses, Mg C ha^{-1} yr^{-1} ‖				
Predictor variable	**Parameter value**	**Standard Error**	**t-value**	**p-value**	**2000-2015 change in losses (%) ***
(Intercept)	1.216	0.086	14.1	<0.001	-
CO_2-change (ppm yr^{-1}) †	0.130	0.059	2.2	0.026	11.38% | 14.81%
MAT-change (°C yr^{-1})	0.766	0.162	4.7	<0.001	-1.56% | 0.00%
MCWD (mm x10000) ‡	-0.232	0.107	-2.2	0.030	-1.21% | -2.42%
CRT (yr)	-0.003	0.001	-6.1	<0.001	-0.57% | 1.39%

* The 2000-2015 change in gains/losses for each predictor variable was estimated allowing only the focal predictor to vary; this change was then expressed as a percentage of the annual gains/losses in the year 2000 allowing all predictors to vary.

† Change over the past 56 years.

‡ Change over the past 5 years.

§ A positive value for Africa indicates that MAT increased more slowly over 2000-2015 compared to the mean increase over 1983-2015, therefore contributing to an increase in gains; a zero value fpr Amazonia indicates that the rate of MAT increase was the same over 2000-2015 as the mean increase over 1983-2015.

‖ Carbon loss values were normalized via power-law transformation, λ= 0.361.

Online Methods

Plot Selection

Closed canopy (i.e. not woody savanna) old-growth mixed-age forest inventory plots were selected using commonly used criteria[6,13,27]: free of fire and industrial logging; all trees with diameter at reference height ≥100 mm measured at least twice; ≥0.2 ha area; <1500 m.a.s.l. altitude; MAT ≥20.0°C[51]; annual precipitation ≥1000 mm[51]; located ≥50 m from anthropogenic forest edges. Of the 244 plots included in the study, 217 contribute to the African Tropical Rainforest Observatory Network (AfriTRON; www.afritron.org), with data curated at www.ForestPlots.net[52,53]. These include plots from Sierra Leone, Liberia, Ghana, Nigeria, Cameroon, Gabon, Republic of Congo, Democratic Republic of Congo (DRC), Uganda and Tanzania[52,53] (Extended Data Figure 1). Fifteen plots are part of the TEAM network, from Cameroon, Republic of Congo, Tanzania, and Uganda[54-57]. Nine plots contribute to the ForestGEO network, from Cameroon and DRC[58] (9 plots from DRC, codes SNG, contribute to both AfriTRON and ForestGEO networks, included above in the AfriTRON total). Finally, three plots from Central African Republic are part of the CIRAD network[59,60]. The large majority of plots are sited in terra firme forests and have mixed species composition, although four are in seasonally flooded forest and 14 plots are in *Gilbertiodendron dewevrei* monodominant forest, a locally common forest type in Africa (Supplementary Table 1). The 244 plots have a mean size of 1.1 ha (median, 1 ha), with a total plot area of 277.9 ha. The dataset comprises 391,968 diameter measurements on 135,625 stems, of which 89.9% were identified to species, 97.5% to genus and 97.8% to family. Mean total monitoring period is 11.8 years, mean census length 5.7 years, with a total of 3,214 ha years of monitoring. The 321 Amazon plots are published and were selected using the same criteria[6], except in the African selection criteria we specified a minimum anthropogenic edge distance and added a minimum temperature threshold.

Plot Inventory and Tree Biomass Carbon Estimation

Tree-level aboveground biomass carbon is estimated using an allometric equation with parameters for tree diameter, tree height and wood mass density[61]. The calculation of each is discussed in turn. All calculations were performed using the R statistical platform, version 3.2.1 (ref.[62]) using the BiomasaFP R package, version 0.2.1 (ref.[63]).

Tree Diameter: In all plots, all woody stems with ≥100 mm diameter at 1.3 m from the base of the stem ('diameter at breast height', DBH), or 0.5 m above deformities or buttresses, were measured, mapped and identified using standard forest inventory methods[64,65]. The height of the point of measurement (POM) was marked on the trees and recorded, so that the same POM is used at the subsequent forest census. For stems developing deformities or buttresses over time that could potentially disturb the initial POM, the POM was raised approximately 500 mm above the deformity. Estimates of the diameter growth of trees with changed POM used the ratio of new and old POMs, to create a single trajectory of growth from the series of diameters at two POM heights[6,13,65]. We used standardised protocols to assess typographical errors and potentially erroneous diameter values (e.g. trees shrinking by >5 mm), missing values, failures to find the original POM, and other issues. Where necessary we estimated the likely value via interpolation or extrapolation from other measurements of that tree, or when this was not possible we used the median growth rate of trees in the same plot, census and size-class, defined as DBH = 100-199 mm, or 200-399 mm, or >400 mm[65]. We interpolated measurements for 1.3% of diameters, extrapolated 0.9%, and used median growth rates for 1.5%.

Tree height: Height of individuals from ground to the top leaf, hereafter H_t, was measured in 204 plots, using a laser hypsometer (Nikon forestry Pro) from directly below the crown (most plots), a laser or ultrasonic distance device with an electronic tilt sensor, a manual clinometer, or by direct

802   measurement, i.e. tree climbing. Only trees where the top was visible were selected[66]. In most plots,

803   tree selection was similar: the 10 largest trees were measured, together with 10 randomly selected

804   trees per diameter from five classes: 100-199 mm, 200-299 mm, 300-399 mm, 400-499 mm, and

805   500+ mm trees, following standard protocols[66]. We measured actual height of 24,270 individual trees

806   from 204 plots. We used these data and the local.heights function in R package BiomasaFP[63] to fit 3-

807   parameter Weibull relationships: $H_t = a \times (1 - e^{((-b \times (DBH/10)^c))})$ (equation 1). We chose the Weibull

808   model as it is known to be robust when a large number of measurements are available[66,67]. We

809   parameterised separate H_t-DBH relationship for four different combinations of edaphic forest type

810   and biogeographical region: (i) terra firme forest in West Africa, (ii) terra firme forest in Lower

811   Guinea and Western Congo Basin, (iii) terra firme forest in Eastern Congo Basin and East Africa,

812   (iv) seasonally flooded forest from Lower Guinea and Western Congo Basin (there were no

813   seasonally flooded forest plots in the other biogeographical regions). The parameters are: (i) terra

814   firme forest in West Africa, a=56.0; b=0.0401; c=0.744; (ii) terra firme forest in Lower Guinea and

815   Western Congo Basin, a=47.6; b=0.0536; c=0.755; (iii) terra firme forest in Eastern Congo Basin

816   and East Africa, a=50.8; b=0.0499; c=0.706; and finally (iv) seasonally flooded forest from Lower

817   Guinea and Western Congo Basin, a=38.2; b=0.0605; c=0.760. For each of these combinations of

818   forest type and bioregion, the local.heights function combines all height measurements from all plots

819   belonging to that forest type/bioregion and fits the Weibull model parameters using non-linear least

820   squares (nls function in R with default settings), with starting values of $a = 25$, $b = 0.05$ and $c = 0.7$

821   chosen as they led to regular model convergence. We fitted these models either treating each

822   observation equally or with case weights proportional to each trees' basal area. These weights give

823   more importance to large trees during model fitting. We selected the best fitting of these models,

824   determining this as the model that minimised prediction error of stand biomass when calculated with

825   estimated heights or observed heights. The parameters were used to estimate H_t from DBH for all

826   tree DBH measurements for input into the allometric equation. Mean measured individual total tree

827 height is 20.5 m; the height range is 1.5 to 72.5 m. The root mean squared error (RMSE) between the

828 full dataset of measured heights and the predicted heights, is 5.7 m, which is 8.0% of the total range.

829 Furthermore, RMSE is 5.3 m in terra firme forest in West Africa (7.5% of the range; n=9771 trees);

830 RMSE is 6.4 m in terra firme forest in Lower Guinea and Western Congo Basin (8.7% of the range;

831 n=10,838 trees); RMSE is 4.8 m in terra firme forest in Eastern Congo Basin and East Africa (8.8%

832 of the range; n=3269 trees); and RMSE is 4.1 m in seasonally flooded forest from Lower Guinea and

833 Western Congo Basin (12.5% of the range; n=392 trees).

834

835 *Wood Density*: Dry wood density (ρ) measurements were compiled for 730 African species from

836 published sources and stored in www.ForestPlots.net; most were sourced from the Global Wood

837 Density Database on the Dryad digital repository (www.datadryad.org)[68,69]. Each individual in the

838 tree inventory database was matched to a species-specific mean wood density value. Species in both

839 the tree inventory and wood density databases were standardized for orthography and synonymy

840 using the African Plants Database (www.ville-ge.ch/cjb/bd/africa/) to maximize matches[13]. For

841 incompletely identified individuals or for individuals belonging to species not in the ρ database, we

842 used the mean ρ value for the next higher known taxonomic category (genus or family, as

843 appropriate). For unidentified individuals, we used the mean wood density value of all individual

844 trees in the plot[13,52].

845

846 *Allometric equation:* For each tree we used a published allometric equation[61] to estimate

847 aboveground biomass. We then converted this to carbon, assuming that aboveground carbon (AGC)

848 is 45.6% of aboveground biomass[70]. Thus: $AGC=0.456\times(0.0673\times(\rho\times(DBH/10)^2\times H_t)^{0.976})/1000$

849 (equation 2), with DBH in mm, dry wood density, ρ, in g cm^{-3}, and total tree height, H_t, in m (ref.[61]).

850

851   *Aboveground Carbon* (AGC, in Mg C ha^{-1}) in living biomass for each plot at each census date was

852   estimated as the sum of the AGC of each living stem, divided by plot area (in hectares).

853

854   **Carbon Gain and Carbon Loss estimation**

855   *Net Carbon Sink* (in Mg C ha^{-1} yr^{-1}) is estimated as carbon gains minus carbon losses. Calculation

856   details are explained below.

857

858   *Carbon Gains* (in Mg C ha^{-1} yr^{-1}) are the sum of the aboveground live biomass carbon additions from

859   the growth of surviving stems and the addition of newly recruited stems, divided by the census

860   length (in years) and plot area (in hectares). For each stem that survived a census interval, carbon

861   additions from its growth (Mg C ha^{-1} yr^{-1}) were calculated as the difference between its AGC at the

862   end census of the interval and its AGC at the beginning census of the interval. For each stem that

863   recruited during the census interval (i.e. reaching DBH≥100 mm), carbon additions were calculated

864   in the same way, assuming DBH=0 mm at the start of the interval[65]. *Carbon Losses* (in Mg C ha^{-1} yr^{-1}

865   ) are estimated as the sum of aboveground biomass carbon from all stems that died during a census

866   interval, divided by the census length (in years) and plot area (in hectares). Both carbon gains and

867   carbon losses are calculated using standard methods[6], including a census interval bias correction,

868   using the SummaryAGWP function of R-package BiomasaFP[63,64,68].

869

870   As carbon gains are affected by a census interval bias, with the underestimate increasing with census

871   length, we corrected this bias by accounting for (i) the carbon additions from trees that grew before

872   they died within an interval (unobserved growth) and (ii) the carbon additions from trees that

873   recruited and then died within the same interval (unobserved recruitment)[65,71].

874

875 Component (i), the unobserved growth of a stem that died during a census interval, is estimated as

876 the difference between AGC at death and AGC at the start of the census. These are calculated using

877 equation 2, from respectively DBH_{death} and DBH_{start}. The latter is part of the data, the first can be

878 estimated as: $DBH_{death} = DBH_{start} \times G \times Y_{mean}$, where G is the plot-level median diameter growth rate

879 (mm yr^{-1}) of the size class the tree was in at the start of the census interval (size classes are defined

880 as D < 200 mm, 400 mm > D ≥ 200 mm and D ≥ 400 mm) and Y_{mean} is the mean number of years

881 trees survived in the census interval before dying. Y_{mean} is calculated from the number of trees that

882 are expected to have died in each year of the census interval, which is derived from the plot-level

883 per-capita mortality rate (m_a; % dead trees yr^{-1}) calculated following equation 5 in ref.[71].

884

885 Component (ii), growth of recruits that were not observed because they died during the census

886 interval, is estimated by calculating the number of unobserved recruits and diameter at death for each

887 unobserved recruit. The number of unobserved recruits (stems ha^{-1} yr^{-1}) is estimated as: $N_{u.r} = R_a -$

888 $P_{surv} \times R_a$, where R_a (recruited stems ha^{-1} yr^{-1}) is the per area annual recruitment calculated following

889 equation 11 in ref.[71] and P_{surv} is the probability of each recruit surviving until the next census: $P_{surv} =$

890 $(1-m_a)^T$, where T is the number of years remaining in the census interval. Summing $N_{u.r}$ for each year

891 in a census interval gives the total number of unobserved recruits in that census interval. We then

892 estimate diameter at death for each unobserved recruit, which is given in mm by $DBH_{death,u.r} = 100 +$

893 $(G_s \times Y_{mean-rec})$, where G_s is the plot-level median diameter growth rate (mm yr^{-1}) of the smallest size

894 class (i.e. D < 200 mm) and $Y_{mean-rec}$ is the mean life-span of unobserved recruits calculated as the

895 mean life-span of recruits in a given year, weighted by $N_{u.r}$. The mean life-span of recruits in a given

896 year is calculated from the number of recruits that died in that year, which is derived from the plot-

897 level per-capita mortality rate (m_a; % dead trees yr^{-1}). Growth of each unobserved recruit (mm yr^{-1}) is

898 then calculated as $DBH_{death,u.r}$ divided by $Y_{mean-rec}$.

899

900   The census interval bias correction (components i and ii together) typically add <3% to plot-level

901   carbon gains. Carbon Losses are affected by the same census interval bias, hence we corrected this

902   bias by accounting for (i) the additional carbon losses from the trees that were recruited and then

903   died within the same interval, and (ii) the additional carbon losses resulting from the growth of the

904   trees that died in the interval[6,15,63]. These two components are calculated in the same way as for

905   Carbon gains and typically add <3% to plot-level carbon losses.

906

907   Carbon gains include both gains from the growth of surviving stems and new recruits. Separating

908   carbon gains from tree growth of surviving stems and newly recruited stems, shows that carbon gains

909   from recruitment are small overall, and are significantly lower in Africa than in the Amazon, likely

910   due to the lower stem turnover rates and longer carbon residence time (Africa: 0.17 Mg C ha^{-1} yr^{-1};

911   CI: 0.16-0.18 versus Amazon: 0.27 Mg C ha^{-1} yr^{-1}; CI: 0.25-0.28, $p<0.001$; two-way Wilcoxon test),

912   but this is compensated by carbon gains from survivors being significantly larger in Africa (2.33 Mg

913   C ha^{-1} yr^{-1}; CI: 2.27-2.39) than in the Amazon (2.13 Mg C ha^{-1} yr^{-1}; CI: 2.09-2.17, $p=0.014$).

914   Therefore, gains overall (sum of gains from surviving stems and newly recruited stems) are

915   indistinguishable between the continents (Africa: 2.57 Mg C ha^{-1} yr^{-1}; CI: 2.51-2.67 vs Amazon: 2.46

916   Mg C ha^{-1} yr^{-1}; CI: 2.41-2.50, $p=0.460$; two-way Wilcoxon test).

917

918   **Long-term Gain, Loss and Net Carbon Sink Trend Estimation, 1983-2014**

919   The estimated mean and uncertainty in carbon gains, carbon losses and the net carbon sink of the

920   African plots from 1983-2014 (Figure 1, Extended Data Figure 7 and Extended Data Figure 8) were

921   calculated following ref.[6] to allow direct comparison with published Amazonian results. First, each

922   census interval value was interpolated for each 0.1-yr period within the census interval. Then, for

923   each 0.1-yr period between 1983 and 2014, we calculated a weighted mean of all plots monitored at

924   that time, using the square root of plot area as a weighting factor[6]. Confidence intervals for each 0.1-

925   yr period were bootstrapped.

926

927   Trends in carbon gains, losses and the net carbon sink over time were assessed using linear mixed

928   effects models (lmer function in R, lme4 package[72]), providing the linear slopes reported in Figure 1.

929   These models regress the mid-point of each census interval against the value of the response variable

930   for that census interval. Plot identity was included as a random effect, i.e. assuming that the intercept

931   can vary randomly among plots. We did not include slope as a random effect, consistent with

932   previously published Amazon analyses[6], because models did not converge due to some plots having

933   too few census intervals. Observations were weighted by plot size and census interval length.

934   Weightings were derived empirically, by assuming *a priori* that there is no significant relation

935   between the net carbon sink and census interval length or plot size, following ref.[13]. The following

936   weighting removes all pattern in the residuals: Weight= $\sqrt[3]{length_{int}}$ + $\sqrt[4]{plotsize}$ -1 (equation 3),

937   where $length_{int}$ is the length of the census interval, in years. Significance was assessed by regressing

938   the residuals of the net carbon sink model against the weights (p=0.702).

939

940   Differences in long-term slopes between the two continents for carbon gains, carbon losses and net

941   carbon sink, reported in the main text, were also assessed using linear mixed effects models, as

942   described above, but performed on the combined African and Amazonian datasets and limited to

943   their common time window, 1983 to 2011.5. For these three tests on the pooled data we included an

944   additional interaction term between census interval date and continent, where a significant

945   interaction would indicate that the slopes differ between continents. The statistical significance of

946   continental differences in slope were assessed using the F-statistic (Anova function in R, car

947   package[73]). Shortening the common time window to the 20 years when the continents are best-

948   sampled, 1991.5 to 2011.5, gave very similar results, including a divergent continental sink (p=0.04).

Continental and Pan-Tropical Carbon Sink Estimates

The *per unit area total net carbon sink* (in Mg C ha^{-1} yr^{-1}) for each time period in Table 1 (each decade between 1980 and 2010; and 2010-2015) is the sum of three components. The first component is the per unit area aboveground carbon sink from living trees and lianas with DBH≥100 mm. For Africa we use the per unit area net carbon sink values presented in this paper. For Amazonia, we use data in ref.[6]. For Southeast Asia, we use inventory data collected using similar standardised methods from 49 plots in ref.[15]. For each time window, we use all plots for which census dates overlap the period, weighted by the square root of plot area, as for the solid lines in Figure 1. The second component is the per unit area aboveground carbon sink from living trees and lianas with DBH<100 mm. This is calculated as 5.19%, 9.40% and 5.46% of the first component (i.e. aboveground carbon of large living trees) in Africa, Amazonia and Southeast Asia respectively[13,74]. The third component is the per unit area belowground carbon sink in live biomass, i.e. roots. This is calculated as 25%, 37% and 17% of the aboveground carbon of living trees with DBH≥100 mm in Africa[13], Amazonia[6] and Southeast Asia[75] respectively.

For each time period in Table 1 we calculated the *continental-scale total carbon sink* (Pg C yr^{-1}) by multiplying the per unit area total net carbon sink described above by the area of intact forest on each continent at that time interval (in ha) reported in Extended Data Table 2. Decades are calculated from 1990.01 to 1999.99. For comparability with previous continental-sink results, we used continental values of intact forest area for 1990, 2000 and 2010 as published in ref.[1], *i.e.* total forest area minus forest regrowth. We used the 1990-2010 data to fit an exponential model for each continent and used this model to estimate intact forest area for 1980 and 2015.

Finally, in the main text we calculated the proportion of anthropogenic CO_2 emissions removed by Earth's intact tropical forests, as the total pan-tropical carbon sink from Table 1 divided by the total anthropogenic

975 CO_2 emissions. Total anthropogenic CO_2 emissions are calculated as the sum of emissions from fossil fuel and

976 land-use change and are estimated at 7.6 Pg C yr^{-1} in the 1990s, 9.0 Pg C yr^{-1} in the 2000s, and 11.1 Pg C yr^{-1}

977 in the 2010s (ref.[21], assuming 1.7% growth in fossil fuel emissions in 2018 and 2019, and mean 2010-2017

978 land-use change emissions for 2018 and 2019).

979

980 **Carbon Sink from an Atmospheric Perspective**

981 To estimate the evolution of the carbon sink from an atmospheric perspective, we assumed that the

982 contribution to the atmosphere from carbon gains are experienced immediately, while the

983 contribution to the atmosphere from carbon losses must take into account the delay in decomposition

984 of dead trees. We did this by calculating total forest carbon loss (Mg C ha^{-1} yr^{-1}) for each year

985 between 1950-2015, using the mean 1983-2015 records from Figure 1 and assuming constant losses

986 prior to 1983 (1.9 and 1.5 Mg C ha^{-1} yr^{-1} for Africa and Amazonia respectively). Then, for each focal

987 year between 1950-2015, we calculated how much carbon was released to the atmosphere in the

988 subsequent years as: $y_t = x_0 \times e^{-0.17 \times (t-1)} - x_0 \times e^{-0.17 \times t}$, where x_0 is the total forest carbon loss of the

989 focal year; y_t is the carbon released to the atmosphere at t years from the focal year; and -0.17 yr^{-1} is

990 a constant decomposition rate calculated for tropical forests in the Amazon[45]. For example, carbon

991 loss was 1.95 Mg C ha^{-1} in 1990 in African forests (Figure 1), from which 0.31 Mg C ha^{-1} was

992 released to the atmosphere in 1991; 0.26 Mg C ha^{-1} in 1992; 0.22 Mg C ha^{-1} in 1993; 0.07 Mg C ha^{-1}

993 in 2000 and 0.01 Mg C ha^{-1} in 2010. Hence, of the full 1.95 Mg C ha^{-1} dead tree biomass from 1990,

994 ~50% was released to the atmosphere after 4 yrs, ~85% after 10 yrs, and ~97% after 20 years.

995 Finally, for each year between 1983 and 2015, the total contribution to the atmosphere from carbon

996 losses was calculated as the sum of all carbon contributions released at that year, from all total yearly

997 forest carbon loss pools of the previous years. We then calculated decadal-scale mean contributions

998 to the atmosphere from carbon losses, reported in the main text.

999

Predictor Variable Estimates, 1983-2014

1000

1001 For each census interval of each plot, we examined potential predictor variables that may explain the

1002 long-term trends in carbon gains and carbon losses, reported in Extended Data Table 1 and main text

1003 Table 2. First, the environmental conditions during the census interval; second the rate of change of

1004 these parameters; and third forest attributes that may affect how different forests respond to the same

1005 environmental change. The predictor variable estimates for each census need to avoid bias due to

1006 seasonal variation, for example the intra-annual variability in atmospheric CO_2 concentration. We

1007 therefore applied the following procedure to avoid seasonal variability impacts on long-term trends:

1008 (i) the length of each focal census interval was rounded to the nearest complete year (e.g. a 1.1 year

1009 interval became a 1 year interval); (ii) we computed dates that minimised the difference between

1010 actual fieldwork dates and complete-year census dates, while ensuring that subsequent census

1011 intervals of a plot do not overlap. The resulting sequence of non-overlapping census intervals was

1012 used to calculate interval-specific means for each environmental predictor variable to remove

1013 seasonal effects. The mean difference between the actual fieldwork dates and the complete-year

1014 census dates is 0.01 decimal years.

1015

1016 The first group of potential predictor variables, estimated for each census interval of each plot, are

1017 theory-driven choices: atmospheric CO_2 concentration (CO_2), mean annual temperature (MAT), and

1018 drought intensity, which we quantified as maximum climatological water deficit (MCWD)[14,20,76,77].

1019

1020 *Atmospheric CO_2 concentration* (CO_2, in ppm) is estimated as the mean of the monthly mean values

1021 from the Mauna Loa record[78] over the census interval. While atmospheric CO_2 concentration is

1022 highly correlated with time (R^2=0.98), carbon gains are slightly better correlated with CO_2

1023 (R_{adj}^2=0.0027) than with time (R_{adj}^2=0.0025).

1024

1025 *Mean Annual Temperature* (MAT, in °C) was derived from the temporally resolved (1901-2015)

1026 dataset of monthly mean temperature from the Climatic Research Unit (CRU TS version 4.03; ~3025

1027 km² resolution; released 15 May 2019; https://crudata.uea.ac.uk/cru/data/hrg/)[79]. We downscaled the

1028 data to ~1 km^2 resolution using the WorldClim dataset[51,80], by subtracting the difference in mean

1029 monthly temperature, and applying this monthly correction to all months[81]. We then calculated MAT

1030 for each census interval of each plot using the downscaled monthly CRU record.

1031

1032 *Maximum Climatological Water Deficit* (MCWD, in mm) was derived from the ~3025 km²

1033 resolution Global Precipitation Climatology Centre dataset (GPCC version 6.0) that includes many

1034 more rain gauges than CRU in tropical Africa[82,83]. As GPCC ends in 2013 we combined it with

1035 satellite-based Tropical Rainfall Measurement Mission data (TRMM 3B43 V7 product, ~757 km²

1036 resolution)[84]. The fit for the overlapping time period (1998-2013) was used to correct the systematic

1037 difference between GPCC and TRMM: GPCC' = a+b*GPCC, with GPCC' the adjusted GPCC

1038 record and a and b different parameters for each month of the year and for each continent.

1039 Precipitation was then downscaled to ~1 km^2 resolution using the WorldClim dataset[51,80], by dividing

1040 by the ratio in mean monthly rainfall, and applying this monthly correction to all months[81]. For each

1041 census interval we extracted monthly precipitation values and estimated evapotranspiration (ET) to

1042 calculate monthly Climatological Water Deficit (CWD), a commonly used metric of dry season

1043 intensity for tropical forests[14,76,77]. Monthly CWD values were calculated for each subsequent series

1044 of 12 months (complete years)[77]. Monthly CWD estimation begins with the wettest month of the first

1045 year in the interval, and is calculated as 100 mm per month evapotranspiration (ET) minus monthly

1046 precipitation (P). Then, CWD values for the subsequent 11 months were calculated recursively as:

1047 $CWD_i = ET - P_i + CWD_{i-1}$, where negative CWD_i values were set to zero[77] (no drought conditions).

1048 This procedure was repeated for each subsequent complete 12 months. We then calculated the annual

1049 MCWD as the largest monthly CWD value for every complete year within the census interval, with

1050   the MCWD of a census interval being the mean of the annual MCWD values within the census

1051   interval. Larger MCWD indicates more severe water deficits.

1052

1053   We assume ET is 100 mm month^{-1} on both continents, based on measurements from Amazonia[76,77],

1054   more limited measurements from West Africa summarized in ref.[85], predictive skill[86], and use in past

1055   studies on both continents[14,87]. MCWD therefore represents a precipitation-driven dry season deficit,

1056   as ET remains constant. An alternative assessment, using a data-driven ET product[88,89], gave a mean

1057   ET of 95 and 98 mm month^{-1} for the African and Amazonian plot networks respectively. Using these

1058   values did not affect the results.

1059

1060   To calculate the environmental change of potential predictor variables, CO_2-change (in ppm yr^{-1}),

1061   MAT-change (in °C yr^{-1}) and MCWD-change (in mm yr^{-1}), we selected an optimum period over

1062   which to calculate the change, derived empirically by assessing the correlation of carbon gains (all

1063   plots, all censuses) with the change in each environmental variable, using linear mixed effects

1064   models (lmer function in R, lme4 package[72]). The annualised change in the environmental variable

1065   was calculated as the change between the focal interval and a prior interval (termed the baseline

1066   period) with a lengthening time window ranging from 1 year through to 80 years prior to the focal

1067   interval (i.e. 80 linear mixed effects models per variable). We calculated AIC for each model and

1068   selected the interval length with the lowest AIC. Thus, MAT-change (in °C yr^{-1}) = $(MAT_i$-

1069 $MAT_b)/(date_i$-$date_b)$, where MAT_i is the MAT over the focal census interval calculated using the

1070   procedure described above, MAT_b is the MAT over a baseline period prior to the focal interval, $date_i$

1071   is the mid-date of the focal census interval and $date_b$ is the mid-date of the baseline period. The lmer

1072   results show that the baseline period for MAT-change is 5 years and for CO_2-change it is 56 years,

1073   while MCWD showed no clear trend, so MCWD-change was not included in the models (see

1074   Extended Data Figure 3). All three results conform to *a priori* theoretical expectations. For CO_2 a

maximum response to an integrated 56 years of change is expected because forest stands will respond most strongly to CO_2 when most individuals have grown under the new rapidly changing condition, which should be at its maximum at a time approximately equivalent to the carbon residence time of a forest stand[30,90] (mean of 62 years in this dataset). For MAT, 5 years is consistent with experiments showing temperature acclimation of leaf- and plant-level photosynthetic and respiration processes over half-decadal timescales[31,91]. MCWD has no overall trend suggesting that once a drought ends, its impact on tree growth fades rapidly, as seen in other studies[14,92]. Also in the moist tropics wet-season rainfall is expected to re-charge soil water, hence lagged impacts of droughts are not expected.

We calculated estimates of two forest attributes that may alter responses to environmental change as potential predictor variables: Wood Density (WD) and Carbon Residence Time (CRT). In intact old-growth forests, mean WD (in $g\ cm^{-3}$) is inversely related to resource availability[28,93,94], as is seen in our dataset (carbon gains and plot-level mean WD are negatively correlated, Extended Data Figure 4). WD is calculated for each census interval in the dataset, as the mean WD of all trees alive at the end of the census interval, to be consistent with the previous Amazon analysis[6]. Carbon residence time (CRT, in yrs) is a measure of the time that fixed carbon stays in the system. CRT is a potential correlate of the impact of past carbon gains on later carbon losses[30]. To avoid circularity in the models, the equation used to calculate CRT differed depending on the response variable. If the response variable is carbon loss, the CRT equation is based on gains: CRT=AGC/gains, with AGC for each interval based on AGC at the end of the interval, and the gains for each interval calculated as the mean of the gains in the interval and the previous intervals (i.e. long-term gains). If the response variable is carbon gains, the CRT equation is based on losses: CRT=AGC/losses. The equation employed for use in the carbon loss model (based on gains) is the standard formula used to calculate CRT and is retained in the minimum adequate model (see below and Table 2). The non-

1100 standard CRT equation (based on losses) used in the carbon gain model is not retained in the

1101 minimum adequate model (see below).

1102

1103 **Statistical modelling of the Carbon Gain, Loss and Sink Trends**

1104 We first constructed two models including those environmental drivers exhibiting long-term change

1105 that impact theory-driven models of photosynthesis and respiration as predictor variables: CO_2,

1106 MAT, and MCWD. One model had carbon gains as the response variable, the other had carbon

1107 losses as the response variable (both in Mg C ha^{-1} yr^{-1}). Models were fitted using the lme function in

1108 R, with maximum likelihood (NLME package[95]). All census intervals within all plots were used,

1109 weighted by plot size and census length (using equation 3 above). Plot identity was included as a

1110 random effect, i.e. assuming that the intercept can vary randomly among plots. All predictor

1111 variables in the models were scaled without centering (scale function in R, RASTER package[62]).

1112 Carbon gain values were normally distributed but carbon loss values required a power-law

1113 transformation (λ= 0.361) to meet normality criteria. Multi-parameter models are: carbon gains =

1114 intcp + a×CO_2 + b×MAT + c×MCWD (model 1); carbon losses = intcp + a×CO_2 + b×MAT +

1115 c×MCWD (model 2); where intcp is the estimated model intercept, and a, b, and c are model

1116 parameters giving the slope of relationships with environmental predictor variables. For multi-

1117 parameter model outputs see Extended Data Table 1, for single-parameter relationships, Figure 2.

1118

1119 The second pair of models include the same environmental predictors (CO_2, MAT, MCWD), plus

1120 their rate of change (CO_2-change, MAT-change, but not MCWD-change as explained above), and

1121 forest attributes that may alter how forests respond (WD, CRT), as described above. We also

1122 evaluated the possible inclusion of a differential continent effect of each variable in the full model.

1123 We first constructed models with only a single predictor variable, and allowed different slopes in

1124 each continent. Next, if removal of the continent-specific slope (using stepAIC function in R, MASS

1125 package[96]) decreased model Akaike Information Criterion (AIC) then the continent-specific slope

1126 was not included in the full model for that variable. Only MCWD showed a significant differential

1127 continent-specific slope. This implies that forests on both continents have common responses to CO_2,

1128 CO_2-change, MAT, MAT-change, WD and CRT, but respond differently to differences in MCWD.

1129 This is likely because wet-adapted species are much rarer in Africa than in Amazonia as a result of

1130 large differences in past climate variation[34]. Lastly, we allowed different intercepts for the two

1131 continents to potentially account for differing biogeographical or other continent-specific factors. For

1132 the carbon loss model, we applied the same continent-specific effects for slope as for the carbon gain

1133 model. Carbon loss values were transformed using a power-law transformation ($\lambda = 0.361$) to meet

1134 normality criteria.

1135

1136 For both carbon gains and losses we parameterized a global model including the significant

1137 continent-specific effect of MCWD, selecting the most parsimonious simplified model using all-

1138 subsets regression[97,98]. To do so, we first generated a set of models with all possible combinations

1139 (subsets) of fixed effect terms in the global model using the dredge function of the MuMIn package

1140 in R[99]. We then chose the best-ranked simplified model based on the AICc criterion, hereafter called

1141 "minimum adequate carbon gain/loss model", reported in Table 2. The minimum adequate models

1142 are: carbon gains = intcp×continent + a×CO_2-change + b×MAT + c×MAT-change +

1143 d×MCWD×continent + e×WD (model 3); carbon losses = intcp + a×CO_2-change + b×MAT-change

1144 + c×MCWD + d×CRT (model 4). WD was retained in the carbon gain model, likely because growth

1145 is primarily impacted by resource availability, while CRT was retained in the carbon loss model,

1146 likely because losses are primarily impacted by how long fixed carbon is retained in the system.

1147

1148 Table 2 presents model coefficients of the best-ranked gain model and best-ranked loss model

1149 selected using all-subsets regression. These best-ranked gain and loss models have weights of 0.310

and 0.132 respectively, which is almost double the weight of the second ranked models (0.152 and

0.075 respectively). In Supplementary Table 2 we also used the model.avg function of the MuMIn

package to calculate a weighted mean of the coefficients of the best-ranked models together

representing a cumulative weight-sum of 0.95 (i.e. a 95% confidence subset). Supplementary Table 2

(model-averaged) and main text Table 2 (best-ranked) model parameters are very similar.

Supplementary Tables 3 and 4 report the complete sets of carbon gains and loss models that

contribute to the model average results.

The model-average results show the same continental differences in sensitivity to environmental

variables as the best-ranked models. From 2000 to 2015, carbon gains increased due to CO_2-change

(+3.7% in both the averaged and the best-ranked models, both continents), while temperature rises

led to a decline in gains, which especially had an effect in the Amazon (-1.14% and -1.07% due to

MAT and MAT-change together in the averaged and best-ranked model respectively). Finally, both

models result in similar predictions of the net carbon sink over the 1983-2040 period: the future net

sink trend in Africa is -0.004 and -0.003 in the best-ranked and averaged models respectively; in

Amazonia the future net sink trend is -0.013 and -0.011 in the best-ranked and averaged models

respectively. The Amazon sink reaches zero in 2041 using model-averaged parameters compared to

2035 using the best-ranked models.

Estimating Future Predictor Variables to 2040

To calculate future modelled trends in carbon gains and losses (Figure 3), we first estimated annual

records of the predictor variables (CO_2-change, MAT, MAT-change, MCWD, WD and CRT) to

2040 (Extended Data Figure 5).

1174   To do so we first calculated annual records for the period of the observed trends for each plot

1175   location (i.e. from 1983-2014 in Africa and 1983-2011.5 in Amazonia). For CO_2-change, MAT,

1176   MAT-change and MCWD we extracted monthly records as described in section Predictor Variable

1177   Estimates (above). For WD and CRT we interpolated to a 0.1-yr period within each census interval

1178   (as in Figure 1). Then, we calculated the mean annual value of each predictor variable from the 244

1179   plot locations in Africa, and separately the mean annual value of each predictor variable from the

1180   321 plot locations in Amazonia (i.e. solid lines in ED Figure 5). For each predictor variable, we

1181   calculated annual records of upper and lower confidence intervals by respectively adding and

1182   subtracting 2σ to the mean of each annual value (shaded area in ED Figure 5).

1183

1184   Secondly, for each predictor variable we parameterised a linear model for each continent using the

1185   annual records for the period of the observed trends. Then for each predictor variable, the continent-

1186   specific linear regression models were used to estimate predictor variables for each plot location

1187   from 2014 to 2040 in Africa and from 2011.5 to 2040 in the Amazon (dotted lines in Extended Data

1188   Figure 5). For each predictor variable, we calculated annual records of upper and lower confidence

1189   intervals by respectively adding and subtracting 2σ to the slope of each linear model (shaded area

1190   around dotted lines in ED Figure 5).

1191

1192   **Estimating Future Carbon Gain, Loss and Net Carbon Sink**

1193   We used the minimum adequate models (Table 2) to predict annual records of carbon gain, carbon

1194   loss and the carbon sink for the plot networks in Africa and Amazonia over the period 1983 through

1195   to 2040 (Figure 3). We extracted fitted carbon gain and loss values using the mean annual records for

1196   each predictor variable (predictSE.lme function, AICcmodavg package[100]). Upper and lower

1197   confidence intervals were calculated accounting for uncertainties in the model (both fixed and

1198   random effects) and predictor variables using the 2σ upper and lower confidence interval for each

1199   predictor variable (using predictSE.lme). Finally the net carbon sink was calculated by subtracting

1200   the losses from the gains. To obtain sink values in the future in Table 1, annual per unit area sink

1201   predictions, from Figure 3, were averaged over each decade and multiplied by the future forest area,

1202   as described above.

1203

1204   To test the sensitivity of the future predictions in Figure 3, we reran the analysis by modifying future

1205   trajectories of predictor variables one at a time, while keeping all others the same, to assess the mean

1206   C sink over 2010-15 and 2030 (averaging at 2030 is not necessary as trends in MAT-change and

1207   MCWD, which largely drive modelled inter-annual variability, are estimated as smooth trends in the

1208   future). For each predictor variable, we explored potential impacts of the likely bounds of possibility,

1209   (i) by taking the steepest slope of either continent from the extrapolated trends, doubling this slope

1210   and applying it on both continents; and (ii) by taking the steepest slope of either continent from the

1211   extrapolated trends, taking the opposite of this slope and applying it on both continents. These

1212   bounds represent deviations of >2 sigma from observed trends. Change in MAT also alters MAT-

1213   change, so we present the sensitivity of both parameters together.

1214

1215   Additionally, for CO_2-change and MAT, we also calculated future slopes under three future

1216   Representative Concentration Pathway (RCP) scenarios[38] with different radiative forcing in 2100:

1217   RCP2.6, 4.5, and 8.5. Future RCP CO_2-change slopes (ppm yr^{-1}) were calculated using RCP CO_2

1218   concentration data for the years between 2015 and 2030 inclusive. Future RCP MAT and MAT-

1219   change slopes were obtained from plot-specific MAT values extracted from downscaled 30 seconds

1220   resolution data for current[80] and future[51] climate from WorldClim, and averaged over 19 CMIP5

1221   models. We subtracted the mean 2040-2060 climate MAT (i.e. 2050) from the mean 1970-2000

1222   climate MAT (i.e. 1985), divided by 65 years to give the annual rate of change. We then calculated a

1223   mean slope over all plots per continent. Finally, to avoid mismatches between RCP-derived values of

1224 CO_2 and MAT and the observed records we removed any difference in intercept between the RCP

1225 trends and observed trends, so the RCP trends were a continuation of the end-point of the observed

1226 trajectory in 2015. We did not estimate the sensitivity of MCWD under the RCP scenarios, because

1227 the CMIP5 model means do not show drought trends for our forest plot networks, unlike rain gauge

1228 data for the recent past, and thus would show little or no sensitivity to MCWD. For each modified

1229 slope, Supplementary Table 5 reports the absolute decline in the sink in each continent in 2030

1230 compared to the 2010-15 mean sink. This shows that the future sink strength is sensitive to future

1231 environmental conditions, but within both RCP scenarios and our bounds of possibility we show a

1232 decline in the sink strength in both continents over the 2020s.

1233

1234 **Data and Code Availability**

1235 Source data and R-code to generate figures and tables are available from:

1236 http://dx.doi.org/10.5521/Forestplots.net/2019_1

1237

1238 **References (Methods only)**

1239 51 Hijmans, R. J., Cameron, S. E., Parra, J. L., Jones, P. G. & Jarvis, A. Very high resolution

1240 interpolated climate surfaces for global land areas. *International Journal of Climatology* **25**,

1241 1965-1978, doi:10.1002/joc.1276 (2005).

1242 52 Lopez-Gonzalez, G., Lewis, S. L., Burkitt, M. & Phillips, O. L. ForestPlots.net: a web

1243 application and research tool to manage and analyse tropical forest plot data. *Journal of*

1244 *Vegetation Science* **22**, 610–613, doi:10.1111/j.1654-1103.2011.01312.x (2011).

1245 53 Lopez-Gonzalez, G., Lewis, S. L., Burkitt, M., T.R., B. & Phillips, O. L. ForestPlots.net

1246 Database. www.forestplots.net. Date of extraction [10/11/2017]. (2009).

1247 54 Sheil, D. & Bitariho, R. Bwindi Impenetrable Forest TEAM Site. Data Set Identifier: TEAM-

1248 DataPackage-20151201235855_1254. (2009).

1249   55   Kenfack, D. Korup National Park TEAM Site. Data Set Identifier: TEAM-DataPackage-
1250   20151201235855_1254. (2011).

1251   56   Rovero, F., Marshall, A. & Martin, E. Udzungwa TEAM Site. Data Set Identifier: TEAM-
1252   DataPackage-20151130235007_5069. (2009).

1253   57   Hockemba, M. B. N. Nouabalé Ndoki TEAM Site. Data Set Identifier: TEAM-DataPackage-
1254   20151201235855_1254. (2010).

1255   58   Anderson-Teixeira, K. J. *et al.* CTFS-ForestGEO: a worldwide network monitoring forests in
1256   an era of global change. *Global Change Biology* **21**, 528-549, doi:10.1111/gcb.12712 (2015).

1257   59   Gourlet-Fleury, S. *et al.* Tropical forest recovery from logging: a 24 year silvicultural
1258   experiment from Central Africa. *Philosophical Transactions of the Royal Society B-*
1259   *Biological Sciences* **368**, 20120302, doi:10.1098/rstb.2012.0302 (2013).

1260   60   Claeys, F. *et al.* Climate change would lead to a sharp acceleration of Central African forests
1261   dynamics by the end of the century. *Environmental Research Letters* **14**, 044002,
1262   doi:10.1088/1748-9326/aafb81 (2019).

1263   61   Chave, J. *et al.* Improved allometric models to estimate the aboveground biomass of tropical
1264   trees. *Global Change Biology* **20**, 3177-3190, doi:10.1111/gcb.12629 (2014).

1265   62   R Development Core Team. R: A Language and Environment for Statistical Computing.
1266   Available at http://www.R-project.org/. (2015).

1267   63   Lopez-Gonzalez, G., Sullivan, M. & Baker, T. BiomasaFP package. Tools for analysing data
1268   downloaded from ForestPlots.net. R package version 0.2.1. Available at
1269   http://www.forestplots.net/en/resources/analysis. (2017).

1270   64   Phillips, O., Baker, T., Brienen, R. & Feldpausch, T. RAINFOR field manual for plot
1271   establishment and remeasurement. Available at
1272   http://www.rainfor.org/upload/ManualsEnglish/RAINFOR_field_manual_version_2016.pdf.
1273   (2016).

1274   65   Talbot, J. *et al.* Methods to estimate aboveground wood productivity from long-term forest

1275   inventory plots. *Forest Ecology and Management* **320**, 30-38,

1276   doi:10.1016/j.foreco.2014.02.021 (2014).

1277   66   Sullivan, M. J. P. *et al.* Field methods for sampling tree height for tropical forest biomass

1278   estimation. *Methods in Ecology and Evolution* **9**, 1179-1189, doi:10.1111/2041-210X.12962

1279   (2018).

1280   67   Feldpausch, T. R. *et al.* Tree height integrated into pantropical forest biomass estimates.

1281   *Biogeosciences* **9**, 3381-3403, doi:10.5194/bg-9-3381-2012 (2012).

1282   68   Chave, J. *et al.* Towards a worldwide wood economics spectrum. *Ecology Letters* **12**, 351-

1283   366, doi:10.1111/j.1461-0248.2009.01285.x (2009).

1284   69   Zanne, A. E. *et al.* *Data from: Towards a worldwide wood economics spectrum* (Dryad

1285   Digital Repository, 2009).

1286   70   Martin, A. R., Doraisami, M. & Thomas, S. C. Global patterns in wood carbon concentration

1287   across the world's trees and forests. *Nature Geoscience* **11**, 915-920, doi:10.1038/s41561-

1288   018-0246-x (2018).

1289   71   Kohyama, T. S., Kohyama, T. I., Sheil, D. & Rees, M. Definition and estimation of vital rates

1290   from repeated censuses: Choices, comparisons and bias corrections focusing on trees.

1291   *Methods in Ecology and Evolution* **9**, 809-821, doi:10.1111/2041-210x.12929 (2018).

1292   72   Bates, D., Maechler, M., Bolker, B. & Walker, S. lme4: Linear mixed-effects models using

1293   Eigen andS4.Rpackage version, 1.0-4. Available at http://www.inside-

1294   r.org/packages/lme4/versions/1-0-4. (2013).

1295   73   Fox, J. *Applied Regression Analysis and Generalized Linear Models*. Second edn, (Sage

1296   Publishing, 2008).

1297   74   Chave, J. *et al.* Assessing evidence for a pervasive alteration in tropical tree communities.

1298   *PLoS Biology* **6**, 0455-0462, doi:10.1371/journal.pbio.0060045 (2008).

1299   75   Yuen, J. Q., Ziegler, A. D., Webb, E. L. & Ryan, C. M. Uncertainty in below-ground carbon

1300   biomass for major land covers in Southeast Asia. *Forest Ecology and Management* **310**, 915-

1301   926, doi:10.1016/j.foreco.2013.09.042 (2013).

1302   76   Aragão, L. E. O. C. *et al.* Spatial patterns and fire response of recent Amazonian droughts.

1303   *Geophysical Research Letters* **34**, 1-5, doi:10.1029/2006gl028946 (2007).

1304   77   Aragão, L. E. O. C. *et al.* Environmental change and the carbon balance of Amazonian

1305   forests. *Biological Reviews* **89**, 913-931, doi:10.1111/brv.12088 (2014).

1306   78   Tans, P. & Keeling, R. Mauna Loa CO_2 monthly mean data. Available at

1307   http://www.esrl.noaa.gov/gmd/ccgg/trends/. (2016).

1308   79   Harris, I., Jones, P. D., Osborn, T. J. & Lister, D. H. Updated high-resolution grids of

1309   monthly climatic observations – the CRU TS3.10 Dataset. *International Journal of*

1310   *Climatology* **34**, 623–642 doi:10.1002/joc.3711 (2014).

1311   80   Fick, S. E. & Hijmans, R. J. WorldClim 2: new 1-km spatial resolution climate surfaces for

1312   global land areas. *International Journal of Climatology* **37**, 4302-4315, doi:10.1002/joc.5086

1313   (2017).

1314   81   Ramirez-Villegas, J. & Jarvis, A. Downscaling Global Circulation Model Outputs: The Delta

1315   Method. Decision and Policy Analysis Working Paper No. 1., 18 (2010).

1316   82   Schneider, U. *et al.* GPCC Full Data Reanalysis Version 6.0 at 0.5°: Monthly Land-Surface

1317   Precipitation from Rain-Gauges built on GTS-based and Historic Data.

1318   doi:10.5676/DWD_GPCC/FD_M_V6_050 (2011).

1319   83   Sun, Q. *et al.* Review of Global Precipitation Data Sets: Data Sources, Estimation, and

1320   Intercomparisons. *Reviews of geophysics* **56**, 79-107, doi:10.1002/ (2017).

1321   84   Huffman, G. J. *et al.* The TRMM Multisatellite Precipitation Analysis (TMPA): Quasi-

1322   Global, Multiyear, Combined-Sensor Precipitation Estimates at Fine Scales. *Journal of*

1323   *Hydrometeorology* **8**, 38-55, doi:10.1175/jhm560.1 (2007).

1324 85 Kume, T. *et al.* Ten-year evapotranspiration estimates in a Bornean tropical rainforest.

1325 *Agricultural and Forest Meteorology* **151**, 1183-1192, doi:10.1016/j.agrformet.2011.04.005

1326 (2011).

1327 86 Zelazowski, P., Malhi, Y., Huntingford, C., Sitch, S. & Fisher, J. B. Changes in the potential

1328 distribution of humid tropical forests on a warmer planet. *Philosophical Transactions of the*

1329 *Royal Society A: Mathematical, Physical and Engineering Sciences* **369**, 137-160,

1330 doi:10.1098/rsta.2010.0238 (2011).

1331 87 James, R., Washington, R. & Rowell, D. P. Implications of global warming for the climate of

1332 African rainforests. *Philosophical transactions of the Royal Society of London. Series B,*

1333 *Biological sciences* **368**, 20120298, doi:10.1098/rstb.2012.0298 (2013).

1334 88 Jung, M. *et al.* Recent decline in the global land evapotranspiration trend due to limited

1335 moisture supply. *Nature* **467**, 951-954, doi:10.1038/nature09396 (2010).

1336 89 Jung, M. *et al.* Global patterns of land-atmosphere fluxes of carbon dioxide, latent heat, and

1337 sensible heat derived from eddy covariance, satellite, and meteorological observations.

1338 *Journal of Geophysical Research* **116**, doi:10.1029/2010jg001566 (2011).

1339 90 Lloyd, J. & Farquhar, G. D. The CO_2 dependence of photosynthesis, plant growth responses

1340 to elevated atmospheric CO_2 concentrations and their interaction with soil nutrient status. I.

1341 General principles and forest ecosystems. *Functional Ecology* **10**, 4-32, doi:10.2307/2390258

1342 (1996).

1343 91 Aspinwall, M. J. *et al.* Convergent acclimation of leaf photosynthesis and respiration to

1344 prevailing ambient temperatures under current and warmer climates in Eucalyptus

1345 tereticornis. *New Phytol* **212**, 354-367, doi:10.1111/nph.14035 (2016).

1346 92 Bonal, D., Burban, B., Stahl, C., Wagner, F. & Hérault, B. The response of tropical

1347 rainforests to drought—lessons from recent research and future prospects. *Annals of Forest*

1348 *Science* **73**, 27-44, doi:10.1007/s13595-015-0522-5 (2016).

1349 93 Quesada, C. A. *et al.* Variations in chemical and physical properties of Amazon forest soils in

1350   relation to their genesis. *Biogeosciences* **7**, 1515-1541, doi:10.5194/bg-7-1515-2010 (2010).

1351 94 Baker, T. R., Swaine, M.D., Burslem, D.F.R.P. Variation in tropical forest growth rates:

1352   combined effects of functional group composition and resource availability. *Perspectives in*

1353   *Plant Ecology, Evolution and Systematics* **6**, 21-36, doi:10.1078/1433-8319-00040 (2003).

1354 95 Pinheiro, J. C. & Bates, D. M. *Mixed-Effects Models in S and S-PLUS.* First edn, 528

1355   (Springer, 2000).

1356 96 Venables, W. N. & Ripley, B. D. *Modern Applied Statistics with S.* Fourth edn, 498

1357   (Springer, 2002).

1358 97 Olejnik, S., Mills, J. & Keselman, H. Using Wherry's Adjusted R^2 and Mallow's Cp for

1359   Model Selection From All Possible Regressions. *The Journal of Experimental Education* **68**,

1360   365-380, doi:10.1080/00220970009600643 (2000).

1361 98 Whittingham, M. J., Stephens, P. A., Bradbury, R. B. & Freckleton, R. P. Why do we still use

1362   stepwise modelling in ecology and behaviour? *Journal of Animal Ecology* **75**, 1182-1189,

1363   doi:10.1111/j.1365-2656.2006.01141.x (2006).

1364 99 Bartoń, K. MuMIn: Multi-Model Inference. Tools for performing model selection and model

1365   averaging. R package version 1.43.6. (2019).

1366 100 Gelman, A. & Hill, J. *Data Analysis Using Regression and Multilevel/Hierarchical Models.*

1367   (Cambridge University Press, New York, 2007).

1368 101 Mayaux, P., De Grandi, G. & Malingreau, J.-P. Central African Forest Cover Revisited: A

1369   Multisatellite Analysis. *Remote Sensing of Environment* **71**, 183–196, doi:10.1016/S0034-

1370   4257(99)00073-5 (2000).

1371

1376

1377   **Extended Data Figures**
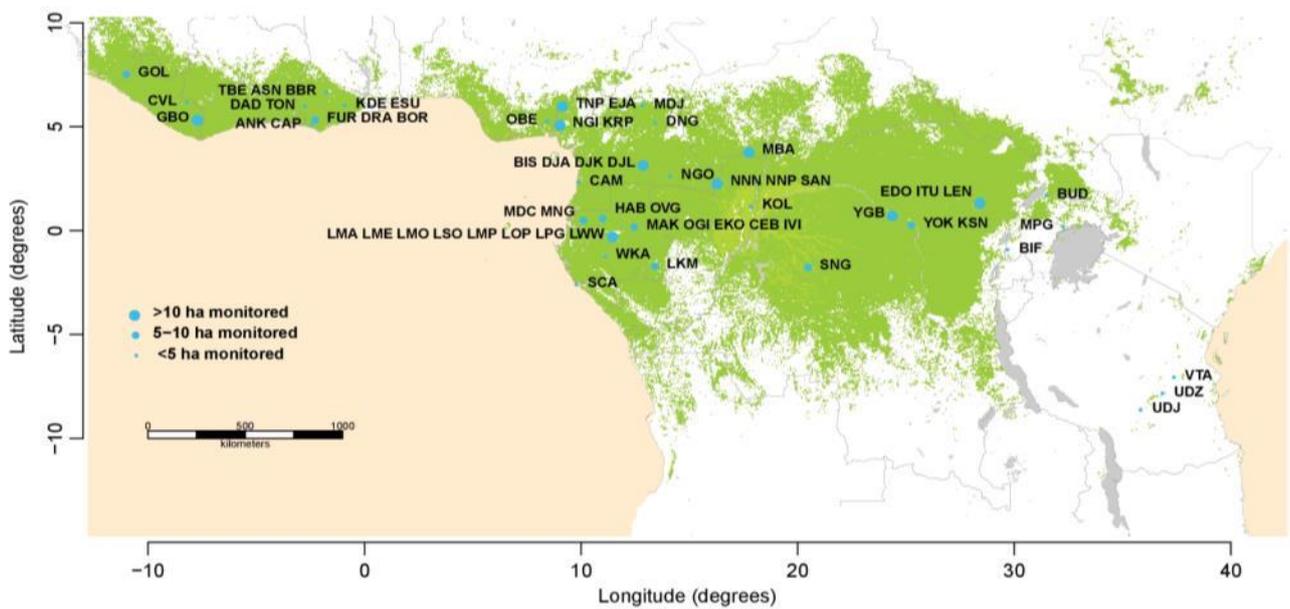
1378

1379   **Extended Data Figure 1. Map showing the locations of the 244 plots included in this study.**

1380   Dark green represents all lowland closed-canopy forests, submontane forests and forest-agriculture

1381   mosaics; light green shows swamp forests and mangroves[101], blue circles represent plot clusters,

1382   referred to by three-letter codes (see Supplementary Table 1 for the full list of plots). Clusters <50

1383   km apart are shown as one point for display only, with the circlesize corresponding to sampling

1384   effort in terms of hectares monitored.
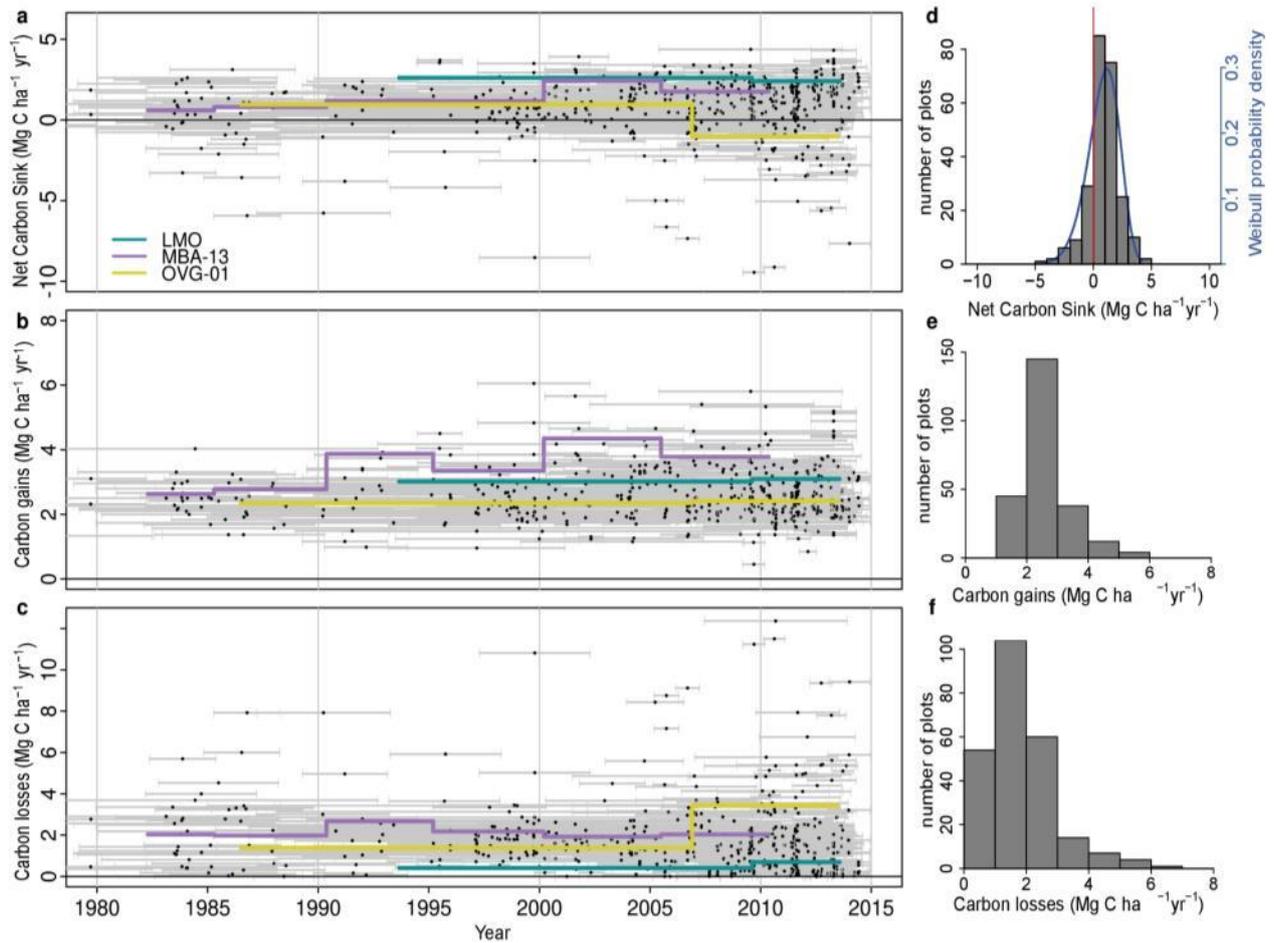
1385

Extended Data Figure 2. Long-term above-ground carbon dynamics of 244 African intact tropical forest inventory plots. Points in the scatterplots indicate the mid-census interval date, with horizontal bars connecting the start and end date for each census interval for net aboveground biomass carbon change (**a**), carbon gains (from woody production from tree growth and newly recruited stems) (**b**), and carbon losses (from tree mortality) (**c**). Examples of time series for three individual plots are shown in purple, yellow and green. Associated histograms show the distribution of the plot-level net aboveground biomass carbon (**d**) (with a three-parameter Weibull probability density distribution fitted in blue, showing the carbon sink is significantly larger than zero; one-tail t-test: p<0.001), carbon gains (**e**), and carbon losses (**f**).
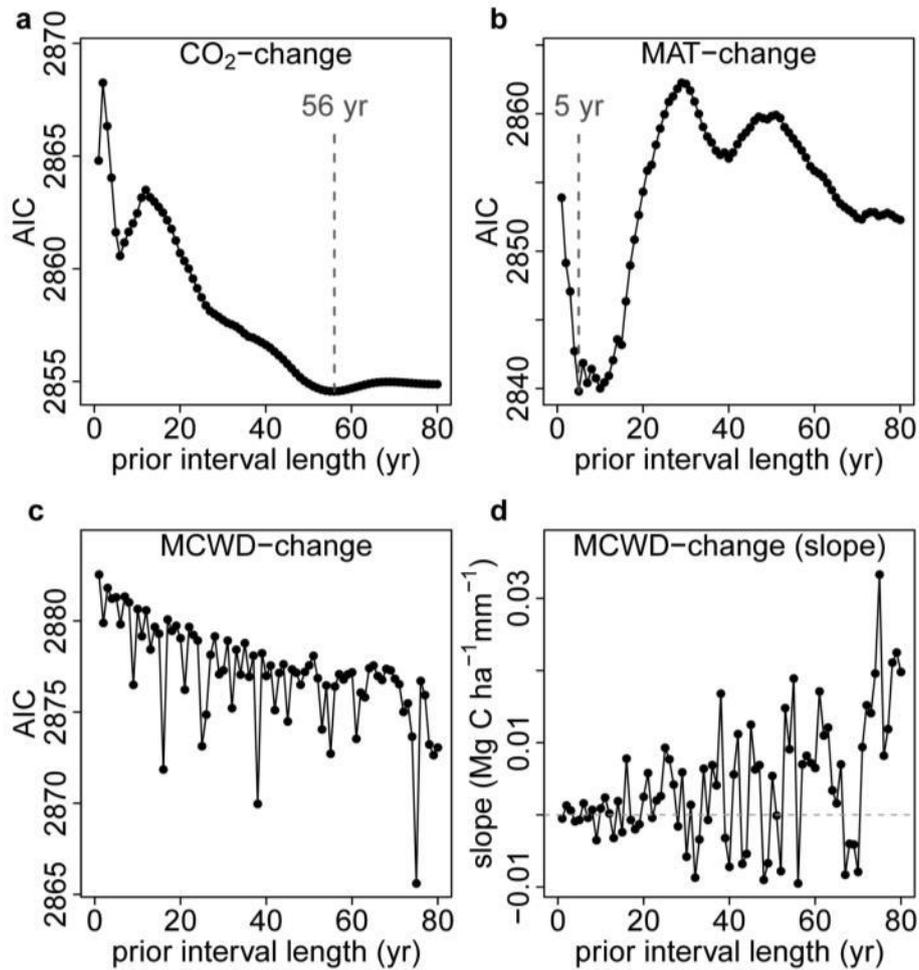
Extended Data Figure 3. Akaike's Information Criterion (AIC) from correlations between the carbon gain in tropical forest inventory plots and changes in either atmospheric CO_2, temperature (as MAT) or drought (as MCWD), each calculated over ever-longer prior intervals. Panels show AIC from linear mixed effects models of carbon gains from 565 plots and corresponding, atmospheric CO_2 (CO_2-change) (**a**), Mean Annual Temperature (MAT-change) (**b**), and Maximum Climatological Water Deficit (MCWD-change) (**c**). For CO_2 the AIC minimum was observed when predicting the carbon gain from the change in CO_2 calculated over a 56 year long prior interval length. We use this length of time to calculate our CO_2-change parameter. Such a value is expected because forest stands will respond most strongly to CO_2 when most individuals have grown under the new rapidly changing condition, which should be at its maximum at a time approximately equivalent to the carbon residence time of a forest stand[30,90] (mean of 62 years in this

1407 pooled African and Amazonian dataset). For MAT the AIC minimum was 5 years, which we use as

1408 the prior interval to calculate our MAT-change parameter. This length is consistent with experiments

1409 showing temperature acclimation of leaf- and plant-level photosynthetic and respiration processes

1410 over approximately half-decadal timescales[31,91]. For MCWD the AIC minimum is not obvious, while

1411 the slope of the correlation, shown in panel (**d**), shows no overall trend and oscillates between

1412 positive or negative values, meaning there is no relationship between carbon gains and the change in

1413 MCWD over intervals longer than 1 year; thus MCWD-change is not included in our models. This

1414 result suggests that once a drought ends, its impact on tree growth fades rapidly, as seen in other

1415 studies[14,92]. Also in the moist tropics wet-season rainfall is expected to re-charge soil water, hence

1416 lagged impacts of droughts are not expected.

1417

1418

1419

1420

1421
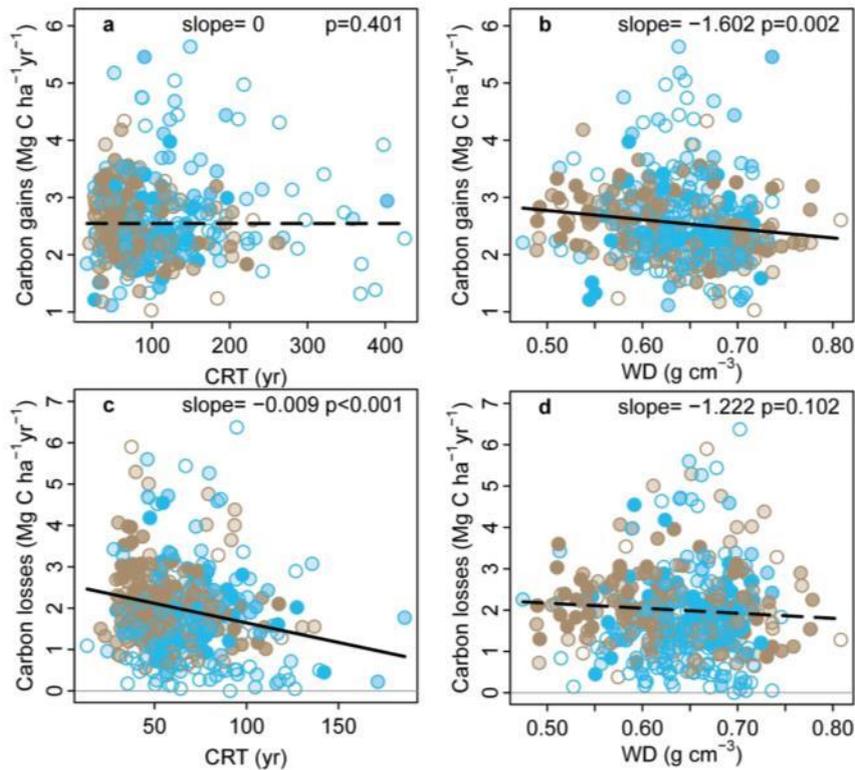
1422

Extended Data Figure 4. Potential forest dynamics-related drivers of carbon gains and losses in structurally intact African and Amazonian tropical forest inventory plots. The aboveground carbon gains, from woody production (**a-b**), and aboveground carbon losses, from tree mortality (**c-d**), are plotted against the carbon residence time (CRT), and wood density (WD), for African (blue) and Amazonian (brown) inventory plots. Linear mixed effect models were performed with census intervals (n=1566) nested within plots (n=565) to avoid pseudo-replication, using an empirically derived weighting based on interval length and plot area (see methods). Significant regression lines for the complete dataset are shown as a solid line; non-significant regressions as a dashed line. Each dot represents a time-weighted mean plot-level value; transparency of the inner part of the dot represents total monitoring length, with empty circles corresponding to plots monitored for ≤ 5 years and solid circles for plots monitored for >20 years. Carbon loss data are presented untransformed for comparison with carbon gains; linear mixed effects models on transformed data to fit normality assumptions do not change the significance of the results. Note, CRT is calculated differently for the carbon gains and losses models (see methods).
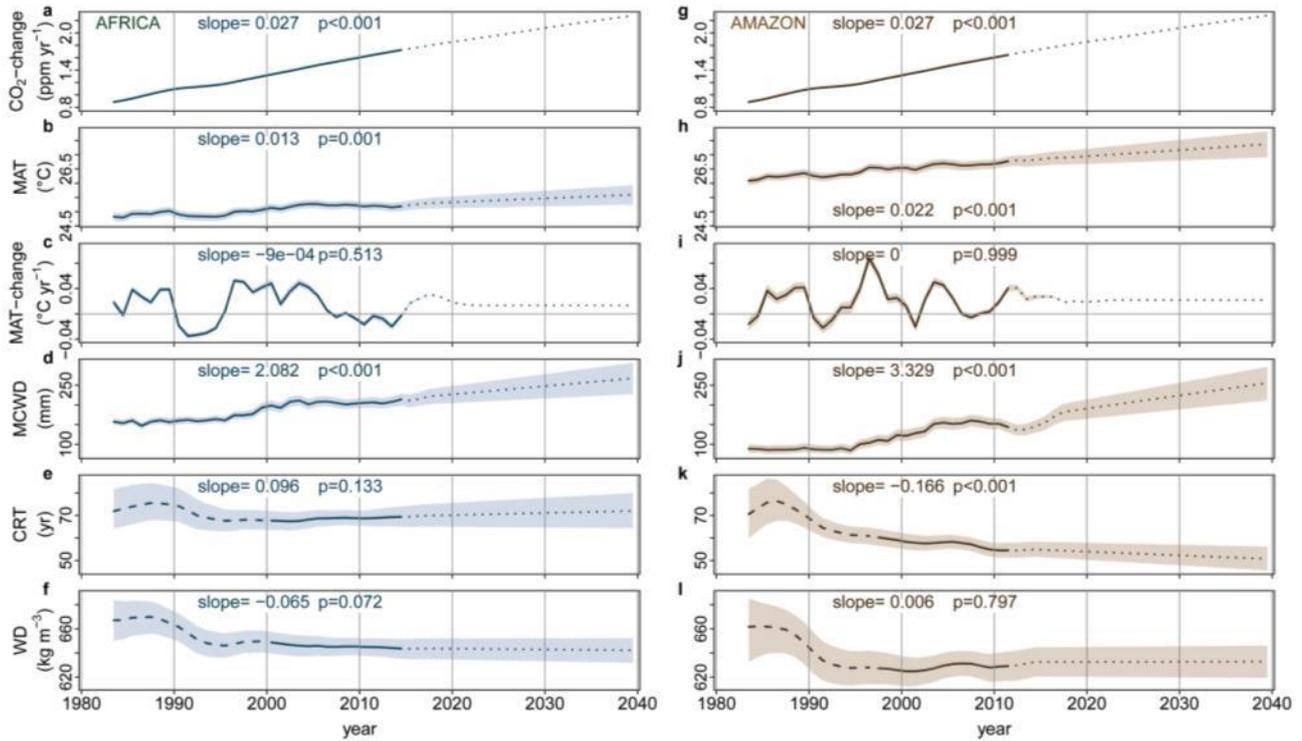
1437

Extended Data Figure 5. Trends in predictor variables used to estimate long-term trends in above-ground carbon gains, carbon losses and the resulting net carbon sink in African and Amazonian intact tropical forest plot networks. Mean annual CO_2-change (**a**), MAT (**b**), MAT-change (**c**), MCWD (**d**), CRT (**e**), and WD (**f**) for African plot locations in blue, and corresponding Amazon plots locations in brown (**g-l**). Solid lines for CO_2-change, MAT, MAT-change, MCWD represent obervational data, and solid lines for CRT and WD represent plot means and a time window where >75% of the plots were monitored, long-dashed lines are plot means were <75% of plots were monitored. Dotted lines are future values estimated from linear trends on the 1983-2014 (Africa) or 1983-2011 (Amazon) data (slope and p-value reported in each panel), see methods for details. Upper and lower confidence intervals (shaded area) for the past (Africa: 1983-2014; Amazonia: 1983-2011) are calculated by respectively adding and subtracting 2σ to the mean of each annual value. Upper and lower confidence intervals for the future were estimated by adding and subtracting 2σ from the slope of the regression model.
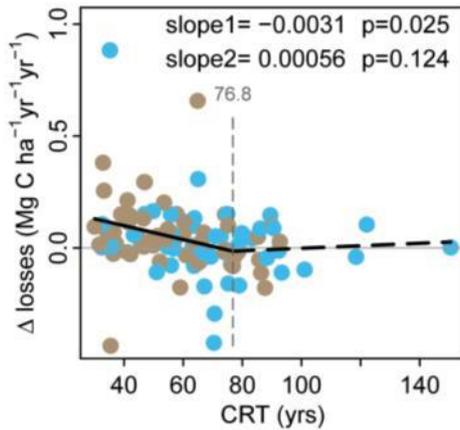
1451

Extended Data Figure 6. The change in carbon losses versus carbon residence time (CRT) of inventory plots in Africa and Amazonia. For plots with two census intervals, we calculated the change in carbon losses (Δlosses, in Mg C ha^{-1} yr^{-1} yr^{-1}) as the carbon losses (Mg C ha^{-1} yr^{-1}) of the second interval minus the carbon losses of the first interval, divided by the difference in mid-interval dates. For plots with more than two intervals, we calculated the change in carbon losses for each pair of subsequent intervals, then calculated the plot-level mean over all pairs, weighted by the time length between mid-interval dates. This analysis includes only plots with at least two census intervals and monitored for $\geq$20 years (i.e. roughly one-third of the mean CRT of the pooled African and Amazon dataset; n = 116). Breakpoint regression was used to assess the CRT length below which forest carbon losses begin to increase. Plots with CRT <77 years show a recent long-term increase in carbon losses, longer CRT plots do not. Blue points are African plots, brown points are Amazonian plots.
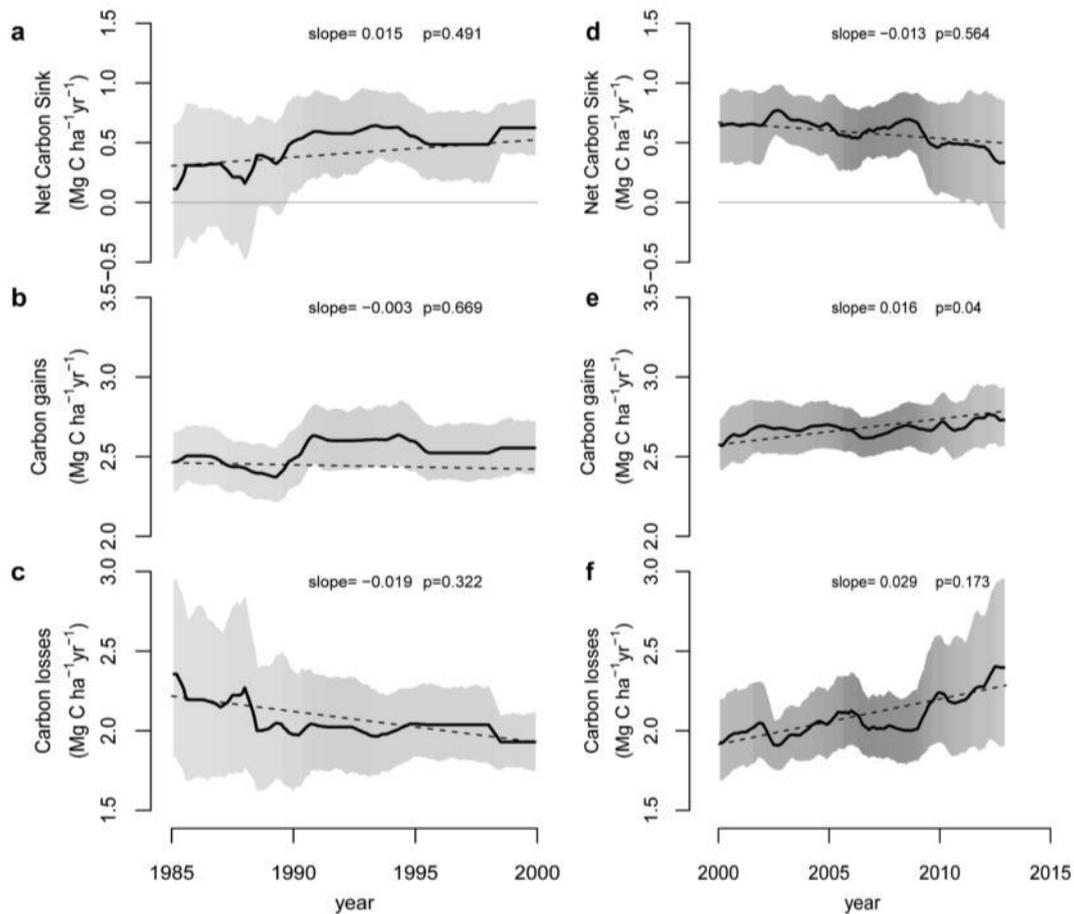
1464

Extended Data Figure 7. Trends in African tropical forest net aboveground live biomass carbon, carbon gains and carbon losses, calculated for the last 15 years of the twentieth century (left panels a-c) and the first 15 years of the twenty-first century (right panels d-f). Plots were selected from the full dataset if their census intervals cover at least 50% of the respective time windows, i.e. they are intensely monitored (n=56 plots for 1985-2000, and n=134 plots for 2000-2015, respectively). Solid lines show mean values, shading corresponds to the 95% CI, as calculated in Figure 1. Dashed lines, slopes and p-values are from linear mixed effects models, as in Figure 1. The data shows a difference compared to Figure 1, notably the sink decline after ~2010 driven by rising carbon losses. This is because in Figure 1 we include all available plots over the 1983-2015 window, which includes clusters of plots monitored *only* in the 2010s that had low carbon loss and high carbon sink values.
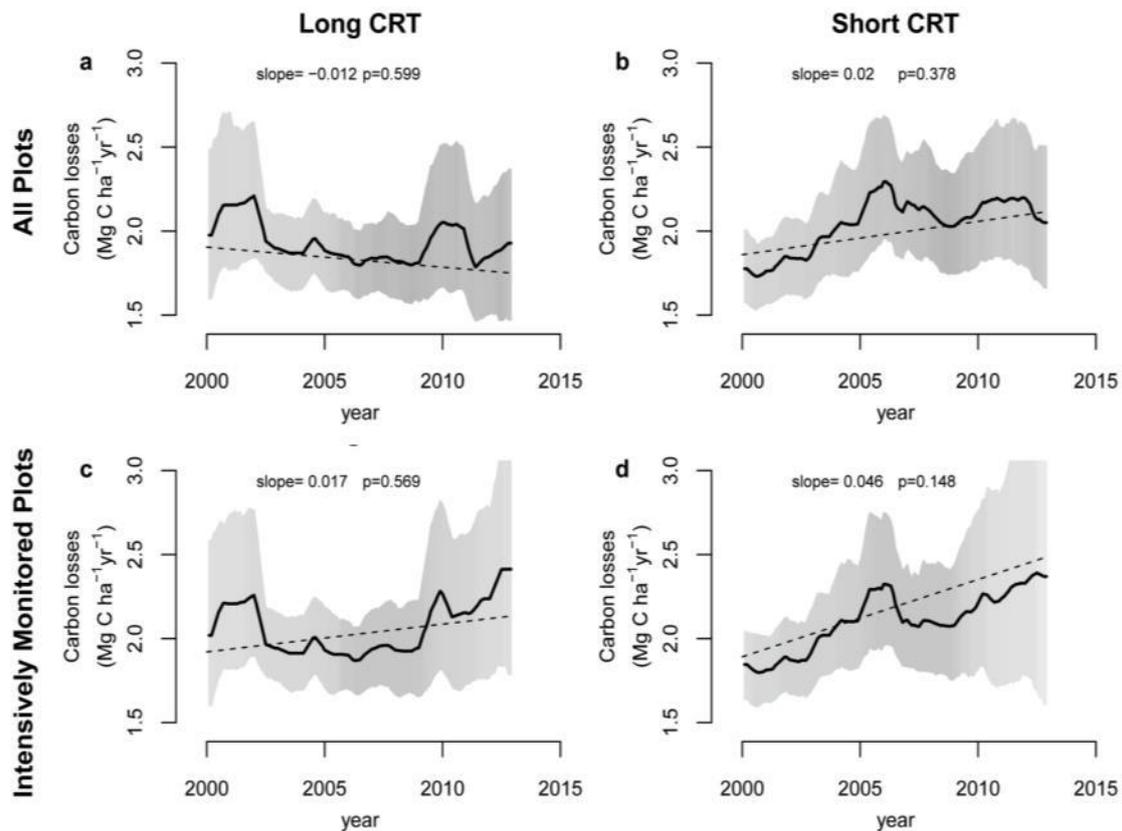
Extended Data Figure 8. Twenty-first century trends in aboveground biomass carbon losses from African tropical forest inventory plots with either long (left panels) or short (right panels) carbon residence time. Upper panels include all plots, i.e. as in Figure 1, but split into a long-CRT group (**a**), and a short-CRT group (**b**), each containing half the 244 plots. Lower panels restrict plots to those spanning >50% of the time window, i.e. intensely monitored plots, as in Extended Data Figure 7, but split into a long-CRT group (**c**), and a short-CRT group (**d**), each containing half the 134 plots. Solid lines indicate mean values, shading the 95% CI, as for Figure 1. Dashed lines, slopes and p-values are from linear mixed-effects models, as for Figure 1. Carbon losses increase at a higher rate in the short-CRT than the long-CRT group of plots, in both datasets, although this increase is not statistically significant.

Extended Data Tables

Extended Data Table 1. Models to predict carbon gains and losses in African and Amazonian

tropical forests, including only environmental variables, showing long-term trends that impact

theory-driven models of photosynthesis and respiration. Significant values in bold.

Carbon gains, Mg C ha^{-1} yr^{-1}				
Predictor variable	Parameter value	Standard Error	t-value	p-value
(Intercept)	4.694	0.739	6.354	0.000
CO_2 (ppm)	**0.005**	0.001	3.196	0.001
MAT (°C)	**-0.143**	0.021	-6.844	0.000
MCWD (mm x1000)	**-1.232**	0.210	-5.878	0.000
Carbon losses, Mg C ha^{-1} yr^{-1} *				
Predictor variable	Parameter value	Standard Error	t-value	p-value
(Intercept)	0.926	1.854	0.500	0.617
CO_2 (ppm)	0.004	0.004	0.947	0.344
MAT (°C)	-0.011	0.044	-0.249	0.804
MCWD (mm x1000)	-0.498	0.505	-0.985	0.325

* carbon loss values were normalized via power-law transformation, λ= 0.361.

Extended Data Table 2. Forest area estimates used to calculate total continental forest sink.

Period	intact forest area (Mha)*			
	Africa	Amazon	Southeast Asia	Pan-tropics
1980	671.5	958.3	233.6	1863.4
1985	634.3	921.1	207.4	1762.8
1990	600.2	885.2	190.6	1676.0
1995	565.9	851.1	163.5	1580.5
2000	531.8	817.2	136.9	1485.9
2005	504.8	784.5	129.2	1418.5
2010	477.8	756.3	118.4	1352.5
2015	450.5	726.7	101.5	1278.7
2020	425.5	698.5	90.1	1214.2
2025	402.0	671.5	80.0	1153.4
2030	379.7	645.4	71.0	1096.1
2035	358.6	620.4	63.0	1042.1
2040	338.8	596.4	56.0	991.1

* Intact forest area for 1990, 2000 and 2007 is published in ref.1 (i.e. the total forest area minus forest regrowth). To estimate intact forest area for the other years in this table, we fitted exponential models for each continent using the published data.